2
Structure of the Ribosome

Gregor Blaha and Pavel Ivanov

Protein synthesis is a complex process with the ribosome as a central player. Its task is to decode the mRNA into the corresponding sequence of amino acids with the aid of amino-acylated tRNAs. We will follow the history of ribosome structure starting with the low-resolution images of the ribosome to arrive at the recent high-resolution, atomic structures for each of the ribosomal subunits, where we will focus on the structural elements that shape them. We will not include detailed structural discussion of 5.5 Å resolution structure of *Thermus thermophilus* 70S [1], since, as Ramakrishnan and Moore [2] emphasized, it is not possible to build a structure *de novo* from a 5.5 Å electron density map. Thus, for example, the structure of the 30S ribosomal proteins in the 70S structure was built by placing those from the 30S subunit structure [3] as rigid bodies into the electron density maps of 70S ribosome [4]. Also the 50S ribosomal subunit of the 70S ribosome structure seems to include some misinterpreted electron density regions. The trace of protein L1 C alpha atoms is partly overlapping with the trace of 23S rRNA phosphorus atoms (PDB code 1 giy) [5, 6] and the orientation of the two domains of L1 deviates from the one observed in L1 [7, 8] or in its complex with rRNA [6].

2.1
General Features of the Ribosome and Ribosomal Subunits

With an approximate mass of 2.6–2.8 MDa the bacterial ribosome has a diameter of 200–250 Å and a sedimentation coefficient of 70S. The 70S ribosome consists of two unequal subunits: a large 50S subunit and a small 30S subunit. Each subunit is a ribonucleoprotein particle with one-third of the mass consisting of protein and the other two-thirds of RNA: a single 16S rRNA (~1500 nt) in the 30S subunit and a 5S (~120 nt) and 23S rRNA (~2900 nt) in the large subunit. The protein fraction consists of approximately 20 different proteins in the small and 33 proteins in the large subunit.

The general outline of the 70S and its component subunits was characterized by a variety of electron microscopic techniques during the 1980s. The 30S was described anthropomorphically with a head, connected by a neck to a body with a shoulder and a so-called platform (Fig. 2-1A). A more compact structure for the 50S was defined, consisting of a rounded base with three almost cylindrical extensions. The three protuberances seen from the 50S side are called from left to right, the L1 protuberance,

Protein Synthesis and Ribosome Structure. Edited by K. H. Nierhaus and D. N. Wilson
Copyright © 2004 WILEY-VCH Verlag GmbH & Co. KGaA, Weinheim
ISBN 3-527-30638-2

the central protuberance, and the L7/L12 stalk (Fig. 2-1B). Both subunits form a 70S ribosome as shown in Fig. 2-1(C). A leap in resolution was achieved by the introduction of single-particle reconstruction of cryo-electron microscopic images [9, 10]. As the resolution improved, the general structural features of the ribosome remained, but more detailed structural features appeared, such as the beak and toe or spur on the 30S (Fig. 2-1A) and a tunnel through the 50S (Fig. 2-1D).

2.2
A Special Feature of the 50S Subunit: The Tunnel

A tunnel transverses the 50S subunit, running from the peptidyl-transferase (PTF) center at the foot of the central protuberance up to the base at the cytoplasmic side of the large subunit with a length of about 100 Å and a width of 10–20 Å (Fig. 2-1D; [11, 10]). The first hint that this tunnel existed was provided by electron microscopy (EM) of two-dimensional (2D) crystals of 80S isolated from chicken embryos [12] and 50S subunits from *Bacillus stearothermophilus* [13]. By that time it had already been shown by immuno-EM that the relative orientation of the exit site of the nascent chain in prokaryotic and eukaryotic ribosomes was identical, located at the lower back (cytoplasmic side) of the large subunit [14]. Moreover, the alignment of cryo-EM structures from rat liver ribosomes with those of *Escherichia coli* proved that not only the central structural features of the ribosome, i.e., L1, L7/L12 and central protuberance, can be superimposed but also the tunnel, suggesting that the tunnel is another universally conserved feature of the ribosome and probably of high functional importance (Fig. 2-1E; [15]). This was subsequently confirmed by the cryo-EM investigations of ribosome–Sec61 complexes from yeast, where the trimeric Sec61 complex, the major component of the endoplasmic pores which conducts the growing nascent peptide chain into the endoplasmic reticulum (ER), was positioned over the exit of the tunnel (Fig. 2-1F; [16]). Recent studies demonstrated that proteins, which are translocated through the ER membrane, indeed exit the ribosome from the ribosomal tunnel [17, 18].

Figure 2-1 Features of the ribosomes. Comparison of ribosomal 30S (A) and 50S subunits (B) and the 70S ribosome (C) from early EM pictures (top row; [104] with the corresponding views obtained by recent cryo-EM reconstructions (bottom row; according to Frank and Agarwal [105]. (D) A cut through the 50S subunit which bisects the central protuberance and the tunnel along the entire length. All ribosome atoms are shown in spacefilling representation, with all RNA atoms that do not contact solvent shown in white and all protein atoms that do not contact solvent shown in green. Surface atoms of both protein and RNA are color-coded: yellow, carbon; red, oxygen; and blue, nitrogen. A possible trajectory for a polypeptide passing through the tunnel is shown as a white ribbon. PT, peptidyl-transferase site [20]. (E) Both the mammalian and the bacterial large subunits have been superimposed. Wherever the bacterial contour lies outside the mammalian one, the resulting surface is gold; wherever the mammalian contour lies outside the bacterial one, the resulting surface is blue. The views are from the 30S subunit side (left) and from the tunnel exit (right). From Ref. [15] with permission. (F) Three-dimensional reconstruction of the ribosome–Sec61 complex with Sec61 oligomer shown in red. Right panel: a cut along a plane that cross sections the pore of the Sec61 oligomer and the ribosome tunnel is shown.

10.1002/3527603433.ch2, Downloaded from https://onlinelibrary.wiley.com/doi/10.1002/3527603433.ch2 by Benjamin Moore - University Of Rhode Island Lib , Wiley Online Library on [04/10/2024]. See the Terms and Conditions (https://onlinelibrary.wiley.com/terms-and-conditions) on Wiley Online Library for rules of use; OA articles are governed by the applicable Creative Commons License

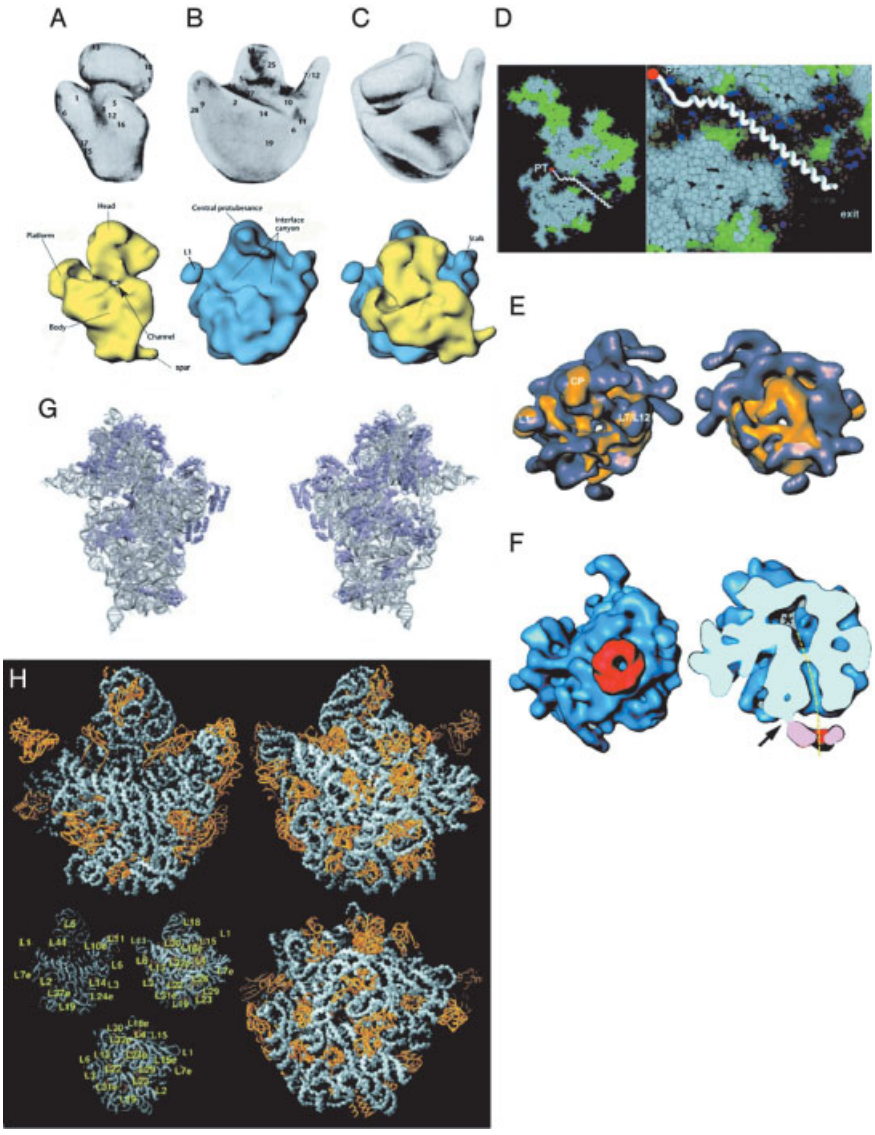

The arrow indicates the stem connecting the ribosome with the Sec61 oligomer; the ribosomal tunnel and its alignment with the Sec61 pore is indicated by a broken yellow line. From Ref. [16], with permission. (G) Distribution of r-proteins in 30S: left seen form the 50S and right the cytosolic side of the 30S. Grey, RNA; blue, proteins. From Ref. [3] with permission. (H) Proteins that appear on the surface of the large ribosomal subunit. The RNA of the subunit is shown in gray and protein backbones are shown in gold. Left panel: the crown view facing the small subunit ; right panel, back side of the subunit (solvent side) in the 180° rotated crown view orientation; bottom right, view from the bottom of the 50S subunit; bottom left, key for the ribosomal proteins. From Ref. [11] with permission.

10.1002/3527603433.ch2, Downloaded from https://onlinelibrary.wiley.com/doi/10.1002/3527603433.ch2 by Benjamin Moore - University Of Rhode Island Lib , Wiley Online Library on [04/10/2024]. See the Terms and Conditions (https://onlinelibrary.wiley.com/terms-and-conditions) on Wiley Online Library for rules of use; OA articles are governed by the applicable Creative Commons License

The 50S crystal structure of *Deinococcus radiodurans* [19] and *Haloarcula marismortui* [11] has now revealed the tunnel at high resolution and confirmed the previously determined dimensions and, furthermore, show that the wall of the tunnel is composed of nucleotides from domains I through V of the 23S rRNA, as well as of the non-globular parts of ribosomal proteins L4 and L22. The narrowest part of the tunnel is formed mainly by ribosomal proteins L4 and L22, where the, β-hairpin of L22 intercalates between rRNA segments of the 23S rRNA. The tunnel surface should minimize unfavorable interactions with growing nascent chains and accordingly no large hydrophobic patches have been observed lining the wall; instead the lining of the tunnel wall is made up of large hydrophilic non-charged groups, thereby facilitating the passage of all kinds of peptide sequences [20]. There seems to exist a system of tunnels, the main tunnel of which represents the shortest route from the entrance to the exterior surface of the ribosome that binds to the bacterial membrane (exit 1), whereas three additional tunnels might communicate with the solvent.

One of these additional routes, which branches off the main tunnel in the segment formed by domains I and III of 23S RNA close to the main exit, was originally discovered at the 25 Å resolution [21]; the branching point is 70 Å away from the tunnel entrance. *H. marismortui* proteins L15 and L29 are closest to the end of this second branch (exit 2; [11]), whose length is 50 Å. Two other branches that start approximately in the same region, which is in fact the widest (20 Å) segment of the main tunnel, partially follow the extensions of proteins L4 (exit 3) and L22 (exit 4). The lengths of these branches from the common branching point to the corresponding exits are approximately 100 and 40 Å, respectively [22, 23]. A similar network of tunnels was also found in *E. coli* ribosomes [22, 23], within the 50S crystal structure of *D. radiodurans* (eubacteria, [19]) and *H. marismortui* (archea, [11]), and in cryo-EM reconstruction of yeast 80S ribosome (eukaryotes, [22, 24]) suggesting that the nascent peptide could in theory emerge into the cytoplasm via one these sub-braches, and thus alternative routes for the nascent peptide chain might be a universal feature of ribosomes.

If the main tunnel is the shortest route and most simple way out of the ribosome, why then does the ribosome need these additional routes branching off the main pathway near the main exit? One possibility is that these openings could maintain the necessary chemical equilibrium in the tunnel system, providing access for water and ion molecules. Another is that they could be used for a more complex regulation of peptide translocation and modification, i.e., the idea being that different polypeptides would utilize different pathways depending on (i) their subcellular destination, (ii) co-factors, e.g., chaperones, which they need for folding or (iii) whether they require post-translational modifications such as methylations, acetylations, or phosphorolations. The implication of this latter view is that the ribosome tunnel would need to play some active role in directing the native peptides in the correct direction. The corollary of this is that there should in fact be specific interactions between the polypeptide and ribosomal components.

This is exactly what a number of recent experiments are clearly indicating: specific peptide sequences have been shown to interact with the interior of the tunnel and

10.1002/3527603433.ch2, Downloaded from https://onlinelibrary.wiley.com/doi/10.1002/3527603433.ch2 by Benjamin Moore - University Of Rhode Island Lib , Wiley Online Library on [04/10/2024]. See the Terms and Conditions (https://onlinelibrary.wiley.com/terms-and-conditions) on Wiley Online Library for rules of use; OA articles are governed by the applicable Creative Commons License

thereby affect protein synthesis on the ribosome. Such sequence-specific interactions between the exit tunnel and nascent peptides suggest that the ribosome, similar to the RNA polymerases [25], can recognize *cis*-acting signals in the synthesized heteropolymeric chain and use them in possibly important intracellular control systems. Nascent peptides in prokaryotes and eukaryotes contain special sequence motifs, and when these effector sequences are situated in the exit tunnel of translating ribosomes, they can significantly affect both protein elongation and peptide termination (Table 2-1) [26, 27]. In all known cases, the peptides with effector motifs act only in *cis* and thus only affect the ribosome on which they are synthesized. Secondly, most effector sequences give rise to ribosomal complexes that are stalled either in the elongation or termination phase of protein synthesis. Thirdly, several of the active peptides have a co-effector and the interplay between an effector motif and a co-effector is key to several intracellular control systems. The co-effector can, for example, be an antibiotic (leading to expression of resistance genes), an amino acid (leading to induction of an amino acid degradation operon), or a polyamine (leading to repression of polyamine synthesis; summarized in Ref. [23]).

An interesting and surprising involvement for the tunnel is in the regulation of a tryptophan catabolite pathway is seen in the expression of the tryptophanase (tna) operon in *E. coli* [28]. Tna is a catabolic enzyme that degrades tryptophan to indole, pyruvate, and ammonia, allowing tryptophan to serve as a carbon or nitrogen source [29]. The tna operon begins with a tnaC gene coding for a 24-amino-acid-long oligopeptide (leader peptide) followed by the structural genes tnaA and tnaB coding for a the tryptophanase and tryptophan permease, respectively [30]. The regulation is orchestrated by the following elements: The 12th and the 24th (last) position of the leader peptide are tryptophan and proline, respectively, followed by the RF2-dependent UGA stop codon. Another set of essential elements include transcriptional pause sites located immediately after the tnaC gene, where Rho-factor-mediated transcription termination can occur and thus prevent synthesis of tryptophanase. First analyses have demonstrated that high tryptophan concentration prevents Rho action [31] and interferes with RF2-dependent hydrolysis [32].

The following mechanism has emerged: The ribosome pursuing the transcriptase during translation of the leader peptide will carry an aa_{23}-Pro-$tRNA^{Pro}$ at its P-site with the 12th Trp residue in the tunnel just where L4/L22 form the kink of the tunnel (see Fig. 2-1D). This constellation with the prolyl residue at the P-site next to the UGA and the tryptophanyl residue at the tunnel kink provokes a stalling of the ribosome and a retardation of the RF2-dependent hydrolysis. At this moment, obviously, the amino acid Trp (not Trp-tRNA!) at high Trp concentration binds to ribosome (possibly to the A-site region of the PTC) thus preventing the hydrolysis of the pp-tRNA and blocking the ribosome on a transcript site of the mRNA required for Rho factor binding. The result is a continuation of transcription into the structural genes tnaA and tnaB fostering the degradation of tryptophan [28].

Another example of a peptide with an effector sequence is the *secM* (secretion monitor) gene of *E. coli* encoding a unique secretory protein that monitors cellular activity for protein export and accordingly regulates translation of the downstream

10.1002/3527603433.ch2, Downloaded from https://onlinelibrary.wiley.com/doi/10.1002/3527603433.ch2 by Benjamin Moore - University Of Rhode Island Lib , Wiley Online Library on [04/10/2024]. See the Terms and Conditions (https://onlinelibrary.wiley.com/terms-and-conditions) on Wiley Online Library for rules of use; OA articles are governed by the applicable Creative Commons License

Table 2-1 **Nascent peptides causing ribosome stalling (data taken from Ref. [23])**

Organism	Gene	Active sequence	Reference	Co-effector	Notes
Eubacteria	cat, cmlA	**MVKTD** **MSTSKNAD**	26	Chloramphenicol	Present in the middle of a small uORF; low concentration of antibiotics cause stalling of the ribosome and therefore rearrangment of mRNA secondary structure releasing the otherwise trapped translation-initiation region of a downstream ORF coding for an enzyme responsible for antibiotic resistance
Eubacteria	ErmC	**SIFVI**	95	Erythromycin	
Eubacteria	TnaC	**KWFNID**	32, 28	Tryptophan	Trp-induced ribosome stalling at the end of a small uORF is essential for attenuation of transcription; ribosome is inhibited at the stage of termination
Eubacteria	secM	**FXXXXWIXXXXGIRAGP**	35	Membrane translocation (secA)	Sensor of protein translocation across the membranes; inhibits translating ribosome; translocation of the nascent chain relieves inhibition
Yeast	CPA1	**NSQYTCQDYISDHIWKTS**	96	Arginine	Small uORFs in the eucaryotic mRNAs cause stalling of the ribosome. This inhibits scanning of the initiation complexes to the main ORF downstream. The Arg-responsible nascent chain CAP1 and arg can act on either terminating or elongating ribosomes. AdoMetDC and CMV UL4 can inhibit termination
Fungi	arg	**PSXFTSQDYXSDHLWXAX**	97	Arginine	
Mammals	AdoMet DC β_2-AdRec Rar- β_2	**MAGDIS** **MKLPGVRPRPAAPRRRCTR** **MIRGWEKDQQPTCQKRGRV**	98–101	Spermidine, spermine	
Mammalian virus	CMV UL4	**MQPLVLSAKKLSSLLTCKY IPP**	102		

10.1002/3527603433.ch2, Downloaded from https://onlinelibrary.wiley.com/doi/10.1002/3527603433.ch2 by Benjamin Moore - University Of Rhode Island Li.b , Wiley Online Library on [04/10/2024]. See the Terms and Conditions (https://onlinelibrary.wiley.com/terms-and-conditions) on Wiley Online Library for rules of use; OA articles are governed by the applicable Creative Commons License

secA gene [33]. SecM is exported to the periplasm, where it is rapidly degraded by a tail-specific protease [34]. The regulation works again via a translational arrest, and, interestingly, with a similar sequence signature as in the previous example: the motif critical for the arrest is FXXXXWIXXXXGIRAGP with a polypeptide Pro-$tRNA^{Pro}$ at the P-site and a Trp residue located 12 aa residues (towards the N-terminal; [35]). This arrest will be only relieved if the ribosomal complex can contact SRP·SecA, thus triggering the export of nascent SecM. Only the stalled ribosome allows the display of the ribosomal binding site for the translation of SecA, whereas relief of the blocked SecM translation allows folding of the secM-secA mRNA, which hides the translational-initiation site of SecA-mRNA region. It follows that a lack of SecA induces synthesis of SecA.

This arrest can be suppressed by each of three amino acid mutations in L22, namely Gly91 to Ser, Ala93 to Thr, and Ala93 to Val. The two residues, 91 and 93, are located on the segment of L22 that protrudes into the exit tunnel at the constricted region. We also see in this example that the regions of L4 and L22 at the tunnel kink (and probably influencing the tunnel shape at this point) might sense the nascent chain in an unknown way, thus influencing essential ribosomal functions occurring not in the adjacent neighborhood such as peptide-bond formation and tRNA translocation.

Modeling of this polypeptide in the tunnel revealed that the conserved Trp-Ile (WI) of the motif would be placed within the most constricted region of the tunnel in close proximity to the tip of the β-hairpin of L22 [36]. Furthermore, the binding of the macrolide troleandomycin with the *D. radiodurans* 50S subunit coincided with this hairpin such that the hairpin was pushed across the tunnel lumen to contact the wall on the other side of the tunnel [36]. This led Yonath and co-workers to suggest that this swung conformation is related to the gating mechanism that is involved in secM-induced translational stalling, i.e., the interaction of the Trp-Ile (both relatively bulky residues) may also induce similar structural rearrangements in L22 such that the tunnel is temporarily closed and therefore translation blocked [36]. Further speculations are that the known ribosomal arrest suppression mutations of L22 (G91S, A93T, and A93V) may stabilize the swung conformation [36]. However, confirmation of this mechanism will require structures of nascent chain-ribosome complexes.

2.3
Features of the Ribosomal Subunits at Atomic Resolution

The first attempts to crystallize the ribosome were undertaken in the 1980s with the first 3D crystals obtained from *B. stearothermophilus* [37]. Owing to continual improvements in the quality of the crystals and in sampling techniques of diffraction patterns (discussed in Ref. [38]), the structure of both subunits at atomic resolution was revealed in the past few years [11, 19, 39, 3].

Although it may not be obvious at first glance, but both large and small subunits have structural features in common at a global as well as at an atomic level. The overall shapes of the atomic resolution structures are in good agreement with those derived from cryo-EM (see Refs. [40, 41] for comparison). The interfaces of both subunits, with the exception of S12 in the small subunit, are essentially protein-free [2],

10.1002/3527603433.ch2, Downloaded from https://onlinelibrary.wiley.com/doi/10.1002/3527603433.ch2 by Benjamin Moore - University Of Rhode Island Lib , Wiley Online Library on [04/10/2024]. See the Terms and Conditions (https://onlinelibrary.wiley.com/terms-and-conditions) on Wiley Online Library for rules of use; OA articles are governed by the applicable Creative Commons License

which had been predicted by neutron scattering [42]. This was later on confirmed by cryo-EM not only for ribosomes from bacteria but also for yeast ribosomes ([43]; see also Fig. 2-1G). In the 50S subunit, the proteins are evenly scattered over the cytosolic surface (Fig. 2-1H), whereas in the 30S they are concentrated mainly in the head and shoulder and platform regions of the body (Fig. 2-1G).

The ribosomal proteins are often bound to junctions between helices, thereby often connecting separate domains, for example S17, which simultaneously contacts helix 7 (h7), h11 of 5′ domain and h21 in the central domain, and L18 which links the helical regions 1 and 2/3 of the 5S rRNA with H87 (note the helices of the rRNA of small ribosomal subunit are denoted with a lower-case letter "h", those of the large subunit with upper-case letter "H" and are counted in the phylogenetically derived secondary structure from the 5′ to 3′ as they occur; see also Sect. 1.4 and Ref. [44]) of 23S rRNA (for helix numbering see below Figs. 2-4A and C; [39, 10, 3]). Many proteins in both subunits have globular domains, generally found on the surface of the subunits, with long extensions that reach far into the RNA core, where they make intimate contacts with the rRNA. These extensions lack tertiary structure and in many regions, even secondary structure, as exemplified by the proteins that neighbor the PTF center (PTC) of the large subunit (Fig. 2-2, [20]). These long extensions from a globular domain represent a new and typical feature of ribosomal proteins and explain the numerous painful and unsuccessful attempts to crystallize many of the ribosomal proteins. A classic example being L2, where only fragments could be crystallized [45], and L4, where crystals were obtained only from a thermophilic bacterium and a halophilic archeon [46]. Almost half of the 30S proteins belong to the category of "globular domain plus long extensions" (such as S2, S6, S9, S11, S12, S14, S16, S17, and protein Thx specifically found in *T. thermophilus*) as well as many of the large subunit proteins (in *H. marismortui*: L2, L3, L4, L15, L18, L19, L22, L24, L37e, L44e, L15e, L37ae and in *D. radiodurans*: L3, L4, L5, L13, L24, L31 (counterpart L15e), L35 (no counterpart in *H. marismortui*)).

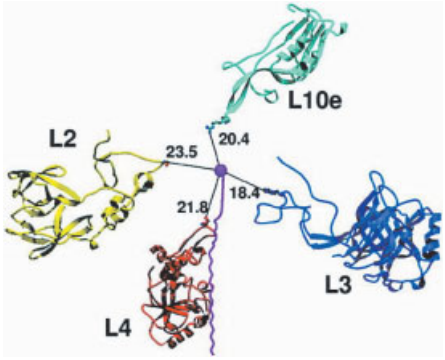

Figure 2-2 A view of the active PTF site with the RNA removed. The proteins with closest extensions to the entrance of the tunnel (pink) through the 50S subunit are shown as ribbons with their closest side chains in all-atom representation. From Ref. [20] with permission.

10.1002/3527603433.ch2, Downloaded from https://onlinelibrary.wiley.com/doi/10.1002/3527603433.ch2 by Benjamin Moore - University Of Rhode Island Lib , Wiley Online Library on [04/10/2024]. See the Terms and Conditions (https://onlinelibrary.wiley.com/terms-and-conditions) on Wiley Online Library for rules of use; OA articles are governed by the applicable Creative Commons License

In the 30S at least, the feature of protein extensions is found only with late-assembly proteins. The large extensions that are rich in basic amino acids (to mask the negative charges of the phosphates in the rRNA backbone) obviously fix the fold of the rRNAs at a late-assembly stage and stabilize the 3D fold of both proteins and rRNAs. In the 50S subunit, the proteins L3, L4, L22, and L25 belong to the proteins that determine a fold of the 23S rRNA essential for the early assembly [47]; in this case they could act initially to connect two distant domains and facilitate their coming together [4].

Even though the general microscopic features, such as the RNA fold or the protein distribution of the different 50S structures, are similar there are some significant differences [19]. For example, the entire L1 stalk in the unbound *D. radiodurans* 50S is tilted by about 30° away from its position in the *T. thermophilus* 70S ribosome yielding a maximum distance of over 30 Å of the outermost points (Fig. 2-3A) [19, 48].

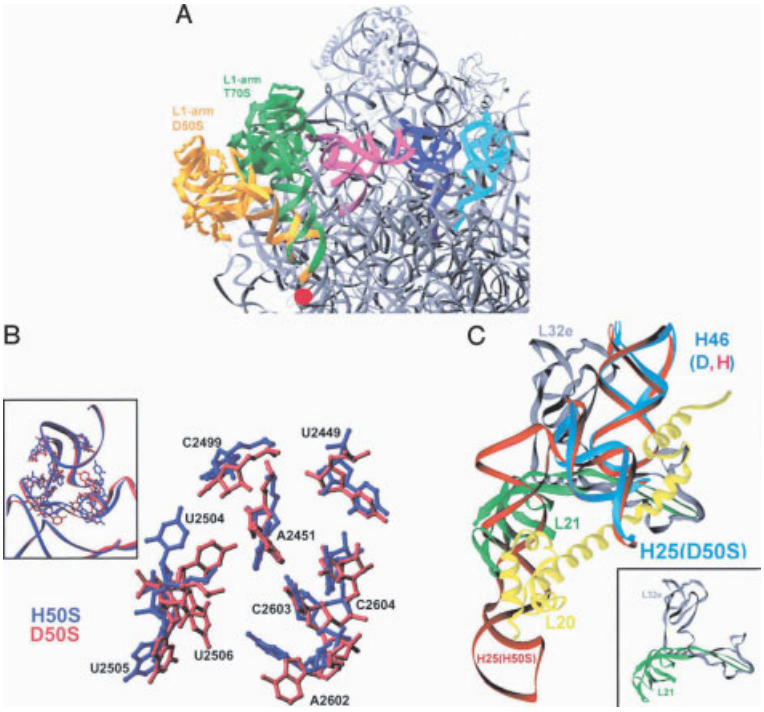

Figure 2-3 Specific features and differences of *D. radiodurans* 50S compared with 50S from *T. thermophilus* 70S and *H. marsimortui* 50S. (A) Movement of L1 stalk. The *D. radiodurans* 50S structure is displayed as gray ribbons with the L1-arm highlighted in gold. The over-laid L1-stalk of T70S is displayed in green. (B) Comparison of the nucleotides within the peptidyl-transferase center of *D. radiodurans* 50S with the corresponding ones from *H. marismortui* 50S. Inset: the overall fold of the peptidyl-transferase center to emphasize the back-bone similarity within *D. radiodurans* and *H. marismortui* 50S. (C) Overlay of H25 in *D. radiodurans* and *H. marismortui* (for details see text). Inset displays proteins L21 and L23e, which are related by an approximate 2-fold. From Ref. [19] with permission.

10.1002/3527603433.ch2, Downloaded from https://onlinelibrary.wiley.com/doi/10.1002/3527603433.ch2 by Benjamin Moore - University Of Rhode Island Lib , Wiley Online Library on [04/10/2024]. See the Terms and Conditions (https://onlinelibrary.wiley.com/terms-and-conditions) on Wiley Online Library for rules of use; OA articles are governed by the applicable Creative Commons License

Also the L7/L12 stalk and the GTPase-associated center consisting of H42–H44 and proteins L7/L12 and L10 are shifted (by 3–4 Å) between *D. radiodurans* 50S and *T. thermophilus* 70S ribosome [1]. The helices H42–H44 show a rotation of about 12° in the case of the *H. marismortui* 50S (PDB 1JJ2) from its position in *D. radiodurans* 50S [19, 48]. These observed flexibilities of the stalks are in line with cryo-EM studies of ribosome complexes in different functional states [49, 50, 24, 51]

H. marismortui 50S crystals derived according to Ban et al. [11] were used in kinetic and crystallographic studies of the PTF reaction. The appearance of peptide product, bound to the PTF ring in the electron density maps of 50S crystal soaked with substrate and the strict dependence of the peptide formation on the presence of 50S crystals clearly demonstrates the catalytic activity of 50S in the disputed crystal form (Refs. [52, 53]; see also Chap. 8.4 on the peptidyl-transferase reaction).

L27, which is located at the base of the central protuberance of *D. radiodurans* and has no homolog in *H. marsimortui*, is proposed to be involved in the proper placement of the 3′-end of the A-site tRNA at the PTC during the PTF reaction [54]. In *H. marismortui,* the non-homologous L21e replaces L27; however, the tail of L21e folds back towards the interior of the subunit and therefore cannot make contact with the P-site tRNA [19].

Other *D. radiodurans*-specific large ribosomal proteins are the L25 analog CTC, which fills the gap between the central protuberance and L7/L12 stalk; the extended α-helical protein L20, which is replaced by 47 n extension in H25 of domain II in *H. marismortui* (see Fig. 2-3C); and the two Zn-finger proteins L32 and L36 [19].

2.4 The Domain Structure of the Ribosomal Subunits

The shear complexity of protein synthesis forces any participating component to maintain their structure and function through evolution. This principle justifies the assumption that not only all tRNAs, but also all 16S (and 16S-like) and 23S (and 23S-like) rRNAs have the same general secondary and tertiary structures [55]. Therefore, the secondary structures of 16S, 23S, and 5S rRNA could be derived by analyzing the pattern of variation within aligned rRNA sequences from different species (see Figs. 2-4A and C; [56]). The resulting secondary-structure diagrams consist of a complex arrangement of A-form helices and non-helical regions (loops or bulges) [55]

In the 16S rRNA the different domains branch from a central pseudo-knot and, beginning from the 5′-end, are termed the 5′, central, 3′-major and 3′-minor domains (see Fig. 2-4A). In striking contrast to the 50S subunit (see following), the domains are not interwoven in the tertiary fold and can be assigned easily to the structural landmarks of the 30S subunit (Fig. 2-4B). The 5′-domain forms the 30S body, starting from the neck of 30S subunit it goes down to the toe and finally turns back to form the shoulder. The central domain constitutes the platform, the 3′-major domain the head. The 3′-minor domain consists of h44 and h45; h44 runs down the 30S along the inter-subunit surface and returns back to the neck, followed by h45 and a single-stranded 3′-end containing the anti-Shine–Dalgarno sequence.

10.1002/3527603433.ch2, Downloaded from https://onlinelibrary.wiley.com/doi/10.1002/3527603433.ch2 by Benjamin Moore - University Of Rhode Island Lib , Wiley Online Library on [04/10/2024]. See the Terms and Conditions (https://onlinelibrary.wiley.com/terms-and-conditions) on Wiley Online Library for rules of use; OA articles are governed by the applicable Creative Commons License

In the 23S rRNA secondary structure the 5′- and 3′-terminal ends are brought together to form a helix (H1 in Fig. 2-4D). Radiating from the loop of this helix are 11 stem-loop structures of differing degrees of complexity. These stem-loop structures

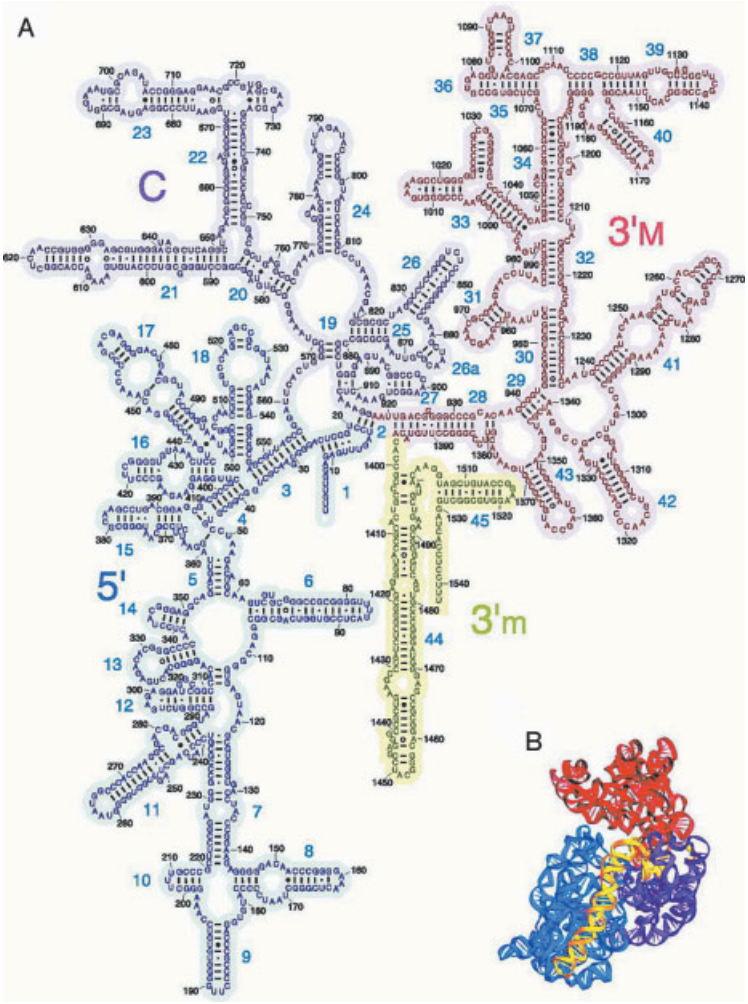

Figure 2-4 Secondary structures of 16S, 23S, and 5S rRNAs. (A) Secondary structure of *T. thermophilus* 16S rRNA, with its 5′, central, 3′-major, and 3′-minor domains shaded in blue, magenta, red, and yellow, respectively. (B) Three-dimensional fold of 16S rRNA in 70S ribosomes, with its domains colored as in (A). (C) Secondary structures of *T. thermophilus* 23S and 5S rRNAs, indicating domains I (blue), II (cyan), III (green), IV (yellow), V (red), and VI (magenta) of 23S rRNA. The rRNAs are numbered according to *E. coli.* (D) Three-dimensional folds of 23S and 5S rRNAs, with their domains colored as in (C).

10.1002/3527603433.ch2, Downloaded from https://onlinelibrary.wiley.com/doi/10.1002/3527603433.ch2 by Benjamin Moore - University Of Rhode Island Lib , Wiley Online Library on [04/10/2024]. See the Terms and Conditions (https://onlinelibrary.wiley.com/terms-and-conditions) on Wiley Online Library for rules of use; OA articles are governed by the applicable Creative Commons License

are bundled into six different domains and, in analogous fashion to the helices, are numbered from the 5′- to 3′-end. The last change in the assignment of the secondary structure to the various domains was contributed by crystallography. Helix 25, which was originally considered as being part of domain I, was reassigned to domain II, because it exhibits stronger interactions with this domain than with the elements of domain I [11]. The six domains of 23S and 5S rRNA all have compact shapes, which are intertwined (Fig. 2-4D). The domains form structural units, as the vast majority of

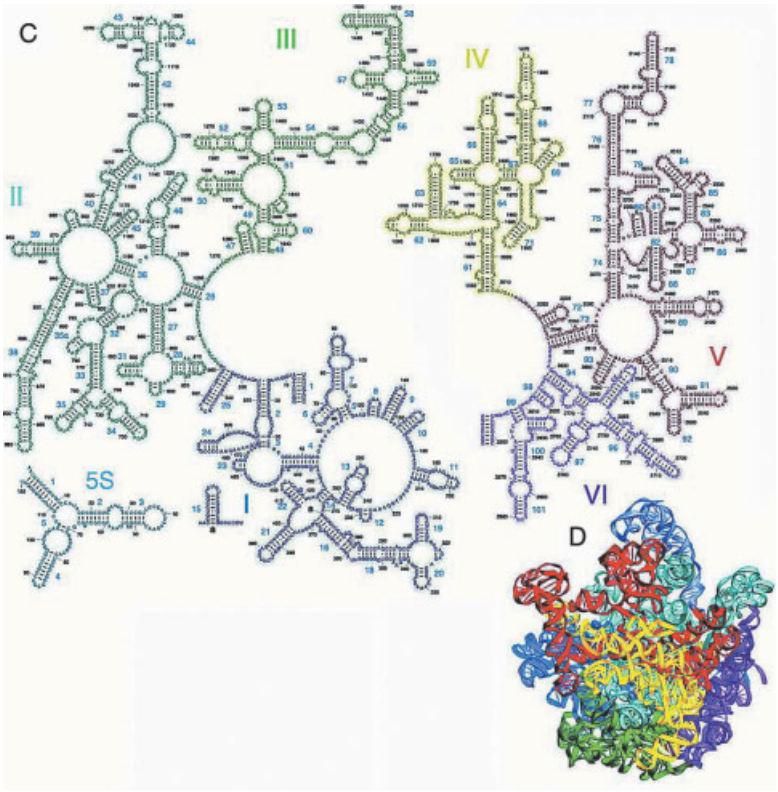

Figure 2-4 From Ref. [1] with permission. (E, F) Comparison of the current comparative structure models for the 16S and 23S rRNAs with the corresponding ribosomal subunit crystal structures. (E) 16S rRNA versus the *T. thermophilus* structure (GenBank accession no. M26923; PDB code 1FJF). (F) 23S rRNA, 5′-half and 3′-half versus the *H. marismortui* structure (GenBank accession no. AF034620; PDB code 1JJ2). Nucleotides are replaced with colored dots that show the sources of the interactions: red, present in both the covariation-based structure model and the crystal structure; green, present in the comparative structure and not present in the crystal structure; blue, not present in the comparative structure and present in the1 crystal structure; purple, positions that are unresolved in the crystal structure.

10.1002/3527603433.ch2, Downloaded from https://onlinelibrary.wiley.com/doi/10.1002/3527603433.ch2 by Benjamin Moore - University Of Rhode Island Lib , Wiley Online Library on [04/10/2024]. See the Terms and Conditions (https://onlinelibrary.wiley.com/terms-and-conditions) on Wiley Online Library for rules of use; OA articles are governed by the applicable Creative Commons License

interactions involving two or more hydrogen bonds occur within domains, rather than between them. This is also the reason for that the interchange of the domain V from *E. coli* against *Staphylococcus aureus* in the 23S rRNA of *E. coli* was possible, even though it introduces 132 changes into the *E. coli* rRNA sequence, only one additional mutation of U1782C for was necessary for viability [57].

Nearly all of the secondary-structure base pairings and a few of the tertiary base pairs observed in the crystal structure had already been predicted by comparative structure models. Specifically, more than 1250 base pairs predicted were indeed present in the 16S and 23S rRNA crystal structures. The ~35 predicted base pairs, which were not found in the crystal structures, could simply not occur at all or possibly only at certain stages of protein synthesis, for example, in the 30S subunit, the A•A base pair between positions 1408 and 1493 is broken upon binding of tRNA and mRNA (cf. 1FJF and 1IBM) [58, 59]. The crystal structures of small and large subunits enriched the secondary-structure diagrams by ~170 base pairs in 16S and ~415 in 23S rRNA, i.e., these were not predicted by comparative methods. Essentially, all the "mis-assigned" base pairs have no significant amount of variation (Ref. [55], see Figs. 2-4E and F).

The fact that the domain secondary structures form well-defined structural domains of quaternary structure in the small subunit, but not in the large subunit, may result from two reasons that need not be mutually exclusive: (i) the small subunit might require larger flexibility for ribosomal functions [2], and the difference in the organization of the secondary structures might indicate that (ii) the 50S subunit is older in evolutionary terms, because more time would be required to evolve such a complicated interwoven structure similar to that of the 50S subunit. As Schimmel and Henderson [60] noted, three elements of protein synthesis, viz. tRNA, synthetases and the ribosome, separate into two domains of different evolutionary ages that have probably co-evolved. The "old" domain of the tRNA is the aminoacyl stem (the short arm of the L-shaped tRNAs or mini-helix), which corresponds to the catalytic domain of synthetases in charging the tRNAs and to the large ribosomal subunit involved in peptide-bond formation. The "young" domains are represented by the long arm of tRNAs bearing the anticodon loop, the recognition domain of the synthetases, and the small ribosomal subunit that interacts with the anticodon loop and some of the stem base-pairs [61, 1].

2.5 Interactions of RNA with RNA or Struts and Bolts in the Three-dimensional Fold of rRNA: Coaxial Stacking and A-minor Motifs

Upon the publication of the structures of the two ribosomal subunits the amount of RNA structure known at atomic resolution increased about 8-fold [62, 2]. However, most of the structure motifs had been seen before, suggesting that the possible number of RNA structure motifs is limited [2]. In this and the following section (2.6), we will restrict our analysis to a specific subsection of structural elements, since tetraloops, tetraloop receptors, adenosine platforms, U-turns, E-loops, sarcin/

10.1002/3527603433.ch2, Downloaded from https://onlinelibrary.wiley.com/doi/10.1002/3527603433.ch2 by Benjamin Moore - University Of Rhode Island Lib , Wiley Online Library on [04/10/2024]. See the Terms and Conditions (https://onlinelibrary.wiley.com/terms-and-conditions) on Wiley Online Library for rules of use; OA articles are governed by the applicable Creative Commons License

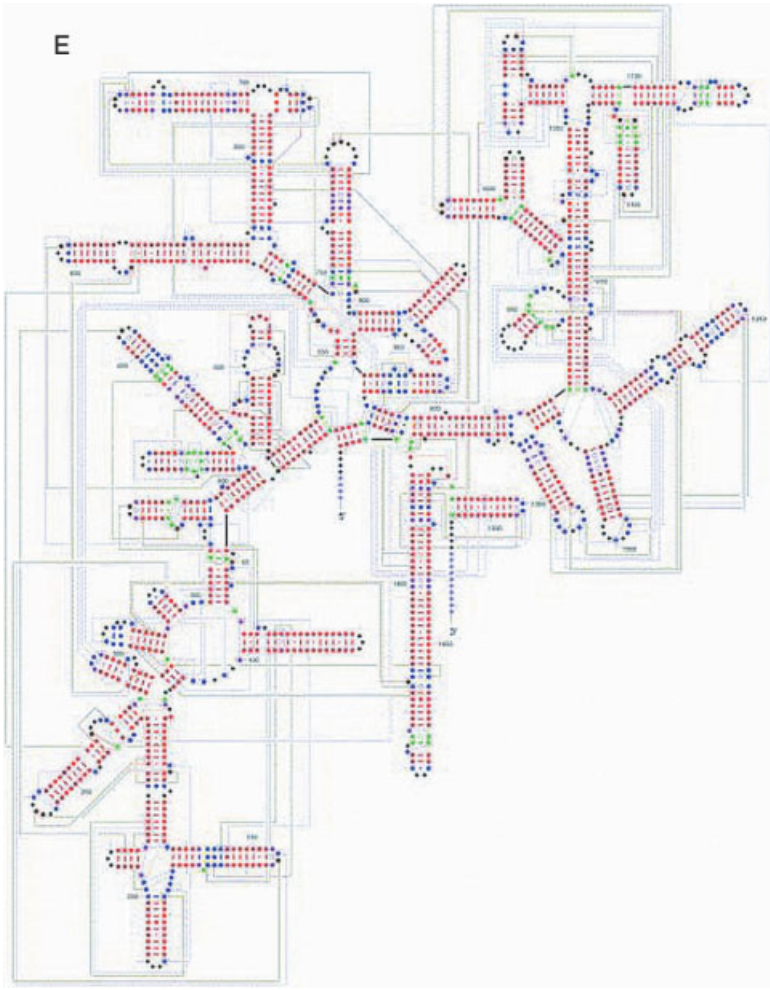

Figure 2-4 (contd.)

ricin motif, and cross-strand purine stacks have been extensively discussed elsewhere [63–66]. In the crystal structure, many of the single-stranded loop regions in the secondary structure turned out to be slightly irregular double-stranded extensions of neighboring regular helices. Thus, most rRNA may be described as helical or approximately helical [3]. These helical elements are organized via vertical co-axial stacking of helices, by A minor interactions and ribose zippers.

2.5.1 Coaxial Stacking

Coaxial stacking is the end-to-end stacking of separate helical RNA parts to form long quasi-continuous helical structures (see as example h16/h17 in 30S or H34/H35 in

10.1002/3527603433.ch2, Downloaded from https://onlinelibrary.wiley.com/doi/10.1002/3527603433.ch2 by Benjamin Moore - University Of Rhode Island Lib , Wiley Online Library on [04/10/2024]. See the Terms and Conditions (https://onlinelibrary.wiley.com/terms-and-conditions) on Wiley Online Library for rules of use; OA articles are governed by the applicable Creative Commons License

Figure 2-4 (contd.)

10.1002/3527603433.ch2, Downloaded from https://onlinelibrary.wiley.com/doi/10.1002/3527603433.ch2 by Benjamin Moore - University Of Rhode Island Lib , Wiley Online Library on [04/10/2024]. See the Terms and Conditions (https://onlinelibrary.wiley.com/terms-and-conditions) on Wiley Online Library for rules of use; OA articles are governed by the applicable Creative Commons License

domain II of 50S in *H. marismortui* [64, 67]). Stacking of nucleic acids is driven by the highly energetically favored stacking interactions between the π-electron system of the nucleic acid bases [68]. The free energy from coaxial stacking of helices ending with Watson–Crick base pairs yields a $\Delta\Delta G^{\circ}$ of –1.0 to –4.5 kcal mol^{-1}, depending on the context. This is in the range of the contribution of next-neighbor interaction to the free energy of an intact helix (–2.0 and –3.4 kcal mol^{-1}) [69, 70]. Also in the same range of free energy is the contribution from coaxial stacking with a single G•A base pair at the interface of the stacking helices (about –2 kcal mol^{-1}, [71]). Therefore, 92% (11/12) of the potential coaxial stacking in the 16S rRNA and 50% (11/22) in the 23S rRNA are observed in the crystal structure. Potential coaxial helix stacking is defined by two helices with an A•G or A•A base-pair at their interface and no unpaired nucleotides in the strand connecting them [58]. Often the A•A and A•G, with the G 3′ to the helix, at the end of helices are inter-convertible.

A good example of a coaxially stacked helix is seen in a classic pseudoknot. This motif consists of a hairpin loop, which base pairs with a complementary single-stranded sequence adjacent to the hairpin stem, to form a contiguous helical structure. Similar to junctions, the coaxial stacking observed in the pseudoknot requires either Mg^{2+} ions or a high concentration of Na^{+} ions for stabilization [63]. Sequence-independent packing of ordinary helices is very seldom seen. It consists of an insertion of a phosphate ridge of one helix into a minor groove of the other at a fixed inter-helical angle of about 80° (e.g., in the 30S subunit for helices h7 and h21 with an angle of 93°). This kind of interaction is already known from the crystal structure of the 59-GGCGCUUGCGUC-39 RNA duplex. In this structure, the duplex forms quasi-continuous helices that pack against each other, with the backbone of one helix in the minor groove of a perpendicular helix [72].

Owing to the limitation to four principal nucleotides, the primary RNA sequence is by itself not enough to define a motif. Moore [66] suggested classifying only structural elements as motifs if they have a defined sequence length or specific loop sizes. This definition would exclude pseudoknots as motifs, as the sequence length and the loop size are unrestricted. Westhof tried to define an RNA motif as an ordered array of stacked non-Watson–Crick base-pairs and thereby focusing plainly on the 3D aspect of a motif. This is well exemplified by the complex topology around G911 in 23S rRNA. The 3D structure of this G911 topology (consisting of nucleotides 1068–1071 and 1292–1295 in one strand and nucleotides 910–914 in the base-pairing strand, shown in red in Fig. 2-5) superimposes well onto the sarcin/ricin motif, as seen in the internal-loop motif G225 in 23S rRNA (shown in blue in Fig. 2-4). The only parts of the motifs that do not superimpose well belong to the backbone, which in the composite motif connects to other parts of 23S RNA [65]. Although this definition of an RNA motif is quite successful, it does not encompasses the K-turn motif, where the array of stacked base pairs is interrupted by a triple loop to introduce a ~120° kink (see below).

As seen above, both secondary- and tertiary-structural aspects must be considered to provide an accurate definition of an RNA motif. In spite of these complications, evidence is accumulating that the modular structure of RNA motifs, which mediate

10.1002/3527603433.ch2, Downloaded from https://onlinelibrary.wiley.com/doi/10.1002/3527603433.ch2 by Benjamin Moore - University Of Rhode Island Lib , Wiley Online Library on [04/10/2024]. See the Terms and Conditions (https://onlinelibrary.wiley.com/terms-and-conditions) on Wiley Online Library for rules of use; OA articles are governed by the applicable Creative Commons License

RNA–RNA (e.g., sarcin/ricin motif [65]) and RNA–protein interactions (e.g., K-turn, see later), are recurrent and are also found in the high-resolution structures of the ribosomal subunits.

2.5.2 A-minor Motifs

From the crystal structure of the *H. marismortui* 50S, the importance of the so-called A-minor motifs for stabilization of the 3D fold of large RNA became evident [73]. Phylogenetic co-variation analysis had already revealed a very strong bias for adenine (A) in single-stranded regions as compared with helical ones, hinting at the important structural or functional role of these adenines (see Table 2-2). One reason for this bias is the crucial importance of A-minor motifs in helix–helix packing, in helix–loop interactions and at helix junctions [73]. In the type-I A-minor motif, the N1-C2-N3 edge of a purine, preferentially a highly conserved A, interacts with the minor groove face of another helix (see Fig. 2-5). The A-minor motif was originally observed in the P4-P6 domain of group I ribozymes, where it was part of the ribose zipper [74], and was subsequently seen in the L11-protein-binding domain of 23S rRNA [75, 76].

Nissen et al. [73] distinguish between four variations in the A-minor motif (types O, I, II and III); however, we will focus primarily on types I and II, as they seem to be the most essential for ribosome function. Examples include the fixation of the CCA end of the tRNA at the PTC [20, 73], A-site recognition of the correct codon–anticodon interaction during the selection of the correct aminoacyl-tRNAs (Fig. 2-6B [59, 77], see also Chaps. 8.2 and 8.4) and subunit association (A702 of 16S rRNA with the minor groove of H68 of 23S rRNA; [1]).

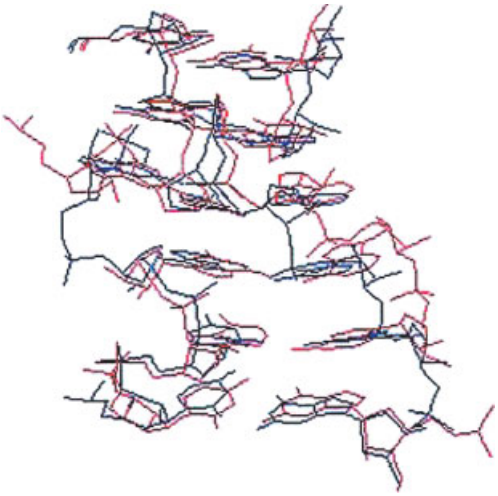

Figure 2-5 Superposition of crystal structures of composite sarcin motif, 23S G911 (red), and internal loop sarcin motif, 23S G225 (blue). From Ref. [65] with permission.

10.1002/3527603433.ch2, Downloaded from https://onlinelibrary.wiley.com/doi/10.1002/3527603433.ch2 by Benjamin Moore - University Of Rhode Island Lib , Wiley Online Library on [04/10/2024]. See the Terms and Conditions (https://onlinelibrary.wiley.com/terms-and-conditions) on Wiley Online Library for rules of use; OA articles are governed by the applicable Creative Commons License

In all A-minor motifs, the ribose-phosphate backbone of the interacting adenosine is closer to one of the strands of the receptor helix. The orientation of the receptor helix strand closest to the adenosine is anti-parallel to the orientation of the adenosine of the donor strand. Type I and II A-minor motifs are different with respect to the position of the 2′-OH and N3 atoms of the adenosine residue relative to the closer strand of the receptor helix (Fig. 2-6; [73]). In type I, both the 2′-OH and the N3 of the adenosine residue are within the minor groove of the receptor helix (Fig. 2-6A), thereby maximizing the number of possible hydrogen bonds to the inserting adenosine. In type II, the N1, C2, N3, and 2′-OH of the adenosine contact approximately half of the minor groove. The 2′-OH of the inserting adenosine is positioned outside of the minor groove with respect to the 2′-OH of the closer strand of the receptor helix, whereas the N3 of the A is inside the minor groove (Fig. 2-6A; [73]). Both types of A-minor motifs are highly specific for adenine bases and show a strong preference for C-G receptor base pairs (Table 2-2; note the preference of adenosine in unpaired regions and the preference of G:C pairs in helices; Fig. 2-6; [73]).

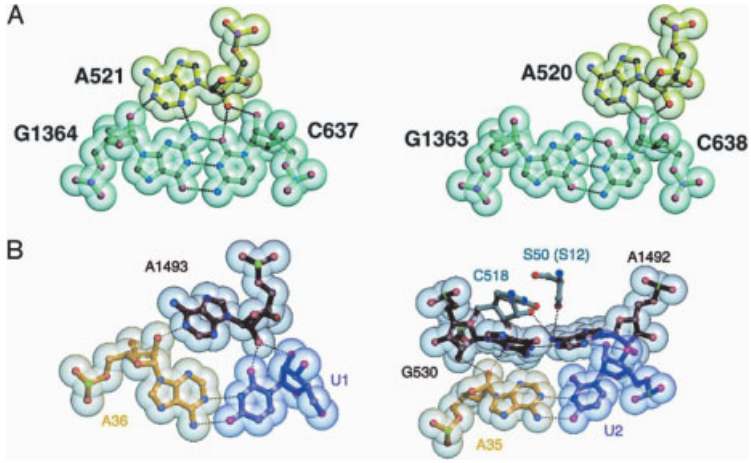

Figure 2-6 A-minor types I and II. (A) Ribosomal examples of A-minor type I and II. Each type is defined by the position of the 2′-OH group of the interacting adenosine relative to the positions of the two 2′-OH groups of the receptor base pair (see text for details). From Ref. [73] with permission. (B) Principles of decoding according to Ref. [59], with permission. For details see text.

Table 2-2 Frequency and distribution % of single nucleotides in bacterial 16S and 23S rRNAs comparative structure models [103]

Nucleotides	G	C	A	U
Overall	31.4	22.4	25.7	20.5
In helices	36.6	28.8	14.8	19.8
In unpaired regions	23.6	12.5	42.6	21.3
Unpaired / total number of positon of nt	30.1	22.3	66.2	41.5

10.1002/3527603433.ch2, Downloaded from https://onlinelibrary.wiley.com/doi/10.1002/3527603433.ch2 by Benjamin Moore - University Of Rhode Island Lib , Wiley Online Library on [04/10/2024]. See the Terms and Conditions (https://onlinelibrary.wiley.com/terms-and-conditions) on Wiley Online Library for rules of use; OA articles are governed by the applicable Creative Commons License

2.5.3 Ribose Zippers and Patches of A-minor Motifs

A ribose zipper is defined as two consecutive hydrogen-bonding interactions between ribose 2′-OH from two different RNA segements. The orientation of the two chains linked by ribose zipper is always antiparallel. A total of 97 ribose zippers are present in the ribosomal subunit crystal structures: 20 in the *T. thermophilus* 16S rRNA, 44 in *H. marismortui* 23S rRNA (plus two ribose zippers bridging 5S rRNA loop E with H38 and the internal loop of H38 and the 5S rRNA helix 4) and 30 in *D. radiodurans* 23S rRNA (plus one bridging 5S and 23S rRNAs) [78]. Out of the 11 possible types of ribose zipper, seven are found in 23S and 16S rRNAs. From these only the canonical and single-base ribose zipper occur more than once in 23S and 16S rRNA [78].

2.5.3.1 Canonical Ribose Zipper

In this type of zipper, the 2′-OH hydrogen bonds are supported by additional hydrogen-bond interactions between the base at the 5′-end and the ribose 2′-OH of the 3′-end on the opposite zipper strand (see Fig. 2-7A). On the base side, the purine N3 or the pyrimidine O2 functions as a hydrogen acceptor. The ribose zipper formed by C376, C377 and A243, A242 in 23S rRNA of *H. marismortui,* has a prototypical topology for the 40 canonical ribose zippers found in the 16S and 23S rRNAs. A243 is inserted into the minor groove of the C376:G274 base-pair forming a type I A-minor motif. A242 interacts via a type II A-minor motif with C377:G273 base pair and is stacked onto A243 (Fig. 2-7B). This tandem A-minor motif seen in 31 instances of the 40 canonical ribose zipper in *T. Thermophilus* 30S and *H. marismortui* 50S had been noticed earlier by Nissen et al. [73], where it was referred to as an "A patch".

The adenosine in the type I A-minor motif, which exhibits stronger conservation than the type II, shows a CG>GC>UA=AU order of preference with regard to the Watson–Crick pairs it interacts with. In contrast, no base-pair preference was detected for the type II A-minor motif [78]. This is in line with experimental and phylogenetic covariation analysis on group I introns [79]. Moreover, with the A-minor patches found in group I introns, the average contribution of the ribose hydrogen bond to the tertiary fold was determined to a $\Delta\Delta G^{\circ}$ of –0.4 to –0.5 [80] and –6.6 kcal/mol^{-1} for type I A-minor motif [79].

2.5.3.2 Single-base Ribose Zipper

The single-base ribose zipper is a canonical ribose zipper with one obstructed base 2′-OH interaction. Two possible types of single-base ribose zippers can be distinguished: types A and B; the definition depending on which base ribose interaction is interrupted, i.e., in either the type I or type II A-minor position, respectively. Consequently, the 15 single-base ribose zippers identified within the *T. thermophilus* 30S and *H. marismortui* 50S can be separated into 10 type A and 5 type B. Almost all single-base ribose zippers have adenine in the type I A-minor position, which is, in the

10.1002/3527603433.ch2, Downloaded from https://onlinelibrary.wiley.com/doi/10.1002/3527603433.ch2 by Benjamin Moore - University Of Rhode Island Lib , Wiley Online Library on [04/10/2024]. See the Terms and Conditions (https://onlinelibrary.wiley.com/terms-and-conditions) on Wiley Online Library for rules of use; OA articles are governed by the applicable Creative Commons License

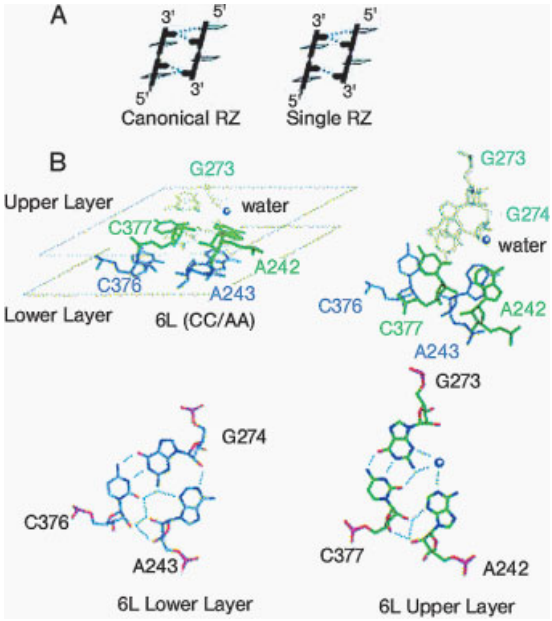

Figure 2-7 Ribose zipper. (A) Schematic representation of canonical and single-base ribose zippers type A. Light blue colored broken lines represent hydrogen bonds. (B) Stick diagrams of the canonical ribose zipper. Top panels: canonical ribose zipper where C377 and A242 belong to the upper layer (blue green) and C376 and A243 belong to the bottom layer (slate) (top left panel) viewed perpendicular to the back-bone, showing the ribose–ribose inter-actions and (top right panel) from above the upper layer. Lower panels: hydrogen-bond network in the lower layer (to the right) and the upper layer (to the left). From Ref. [78] with permission.

case of type A, rotated away from the "acceptor base pair". In the type B single-base ribose zipper the type II A-minor position is a G in all instances [78]. Comparison of the two available 50S structures revealed that 10 of the canonical ribose zippers that are present in *H. marismortui* are also found in *D. radiodurans*, although two canonical ribose zippers in *H. marismortui* are single-base ribose zippers in *D. radiodurans*.

All ribose zippers of *H. marismortui* 50S structure are either conserved or their composing bases are in close proximity to each other in *D. radiodurans* structure. For example, 10 *canonical ribose zippers* found specifically in *H. marismortui* have similar positions in *D. radiodurans*; however, the bases are too far apart from each other to form hydrogen bonds.

2.6 Progress and New Developments in Understanding rRNA Structures

To finalize the overview of motifs recognized in the ribosomal subunit, the K-turn and lonepair triloop will be reviewed as well as the attempts that have been made to categorize non-Watson–Crick base interactions and RNA motifs in databases.

10.1002/3527603433.ch2, Downloaded from https://onlinelibrary.wiley.com/doi/10.1002/3527603433.ch2 by Benjamin Moore - University Of Rhode Island Lib , Wiley Online Library on [04/10/2024]. See the Terms and Conditions (https://onlinelibrary.wiley.com/terms-and-conditions) on Wiley Online Library for rules of use; OA articles are governed by the applicable Creative Commons License

2.6.1
K-turn

After careful analysis of crystal structure of the large subunit, Klein et al. [62] recognized a new motif, consisting of a helix–internal loop–helix. A kink in the phosphodiester backbone of the internal loop bends the RNA helix axis by ~120° and also gives the motif its name 'Kink-turn' or 'K-turn'.

The first helical stem termed 'canonical stem' (C-stem) ends at the internal loop with two Watson–Crick base pairs, typically C:Gs. The second helical stem termed 'non-canonical stem' (NC-stem) follows the internal loop and starts with two non-Watson–Crick base pairs, typically sheared G•A base pairs. The internal loop between the helical stems is always asymmetrical and usually contains three unpaired nucleotides in one strand but none in the other (Fig. 2-8A). The close helical packing between the helical stems is stabilized by a type I A-minor interaction [73] between the last C:G of the C-stem and the A of the G•A base pair in the NC-stem (Fig. 2-8B). The requirement for a type I A-minor interaction may account for the conservation of C:G in the C-stem and A•G in the NC-stem and also the high conservation with the consensus secondary structure for the K-turn, which includes 10 consensus nucleotides out of the possible 15 [62]. Although the eight K-turns identified in the *H. marismortui* 23S and *T. thermophilus* 16S rRNA vary somewhat in sequence, each has essentially the same distinctive 3D structure. The six K-turns in *H. marismortui* 23S rRNA superimpose with an r.m.s.d. of 1.7 Å (r.m.s.d.: root-mean-square deviation). All six of these K-turn motifs appear at or near the surface of the 50S particle, in regions that are less well conserved among the three kingdoms (Fig. 2-8C). The two K-turns identified in the structure of *T. thermophilus* 30S are localized in the intersubunit surface and probably play a structural role in the association of the subunits.

2.6.2
Lonepair Triloop

As implied in the name, the lonepair triloop (LPTL) consists of a lone base pair capped with a loop of three nucleotides. The nucleotide sequence within LPTLs can be described as 5′–FXYZL–3′, where the underlined nucleotides F and L form the lonepair and the three nucleotides, X, Y and Z, the triloop [81]. Twenty-three LPTLs occur in the ribosomal RNAs, of which seven are in 16S rRNA of *T. thermophilus* 30S, 15 in the 23S and one in 5S rRNA of the *H. marismortui* 50S. The LPTLs in *D. radiodurans* 50S are at the corresponding positions of 23S RNA of *H. marismortui* and are structurally equivalent. In addition to the LPTLs recognized in the ribosomal RNA an additional one was found in the T-loop of tRNAs [81]. Nearly all of the LPTL sites in rRNAs are conserved and most of them contribute to rRNA packing via tertiary interactions with RNA segments that are distant in terms of the secondary structure [81].

10.1002/3527603433.ch2, Downloaded from https://onlinelibrary.wiley.com/doi/10.1002/3527603433.ch2 by Benjamin Moore - University Of Rhode Island Lib , Wiley Online Library on [04/10/2024]. See the Terms and Conditions (https://onlinelibrary.wiley.com/terms-and-conditions) on Wiley Online Library for rules of use; OA articles are governed by the applicable Creative Commons License

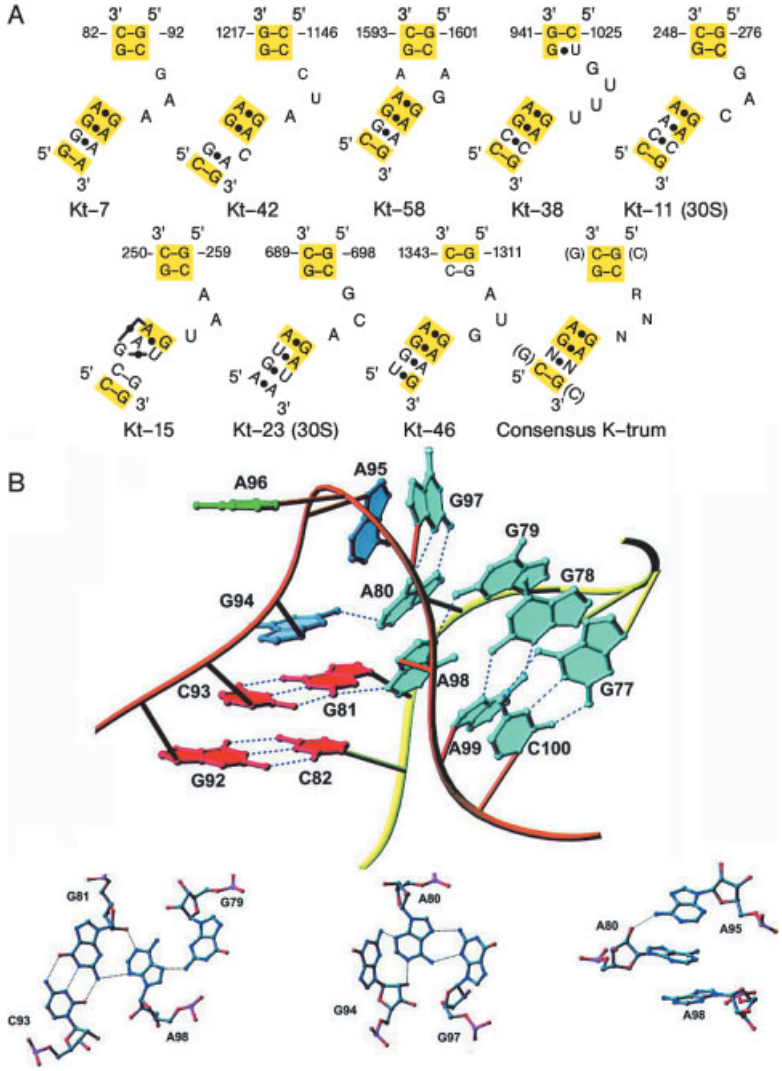

Figure 2-8 K-turn motif. (A) Secondary-structure diagrams of the eight K-turns found in the *H. marismortui* 50S and *T. thermophilus* 30S subunit structures and a derived consensus sequence. (B) Three-dimensional representation of KT-7 with the phosphate backbone of the kinked strand in orange and the unkinked strand in yellow (upper panel). Lower panels displays atomic details of individual base–base and base–backbone hydrogen bonds. (C) Location of the K-turns in the *H. marismortui* 50S structure. K-turns in blue are shown in the 3D structure: crown view from the interface (top left panel), cytosolic face (top right panel) and in the secondary structure (lower panel). From Ref. [62] with permission.

10.1002/3527603433.ch2, Downloaded from https://onlinelibrary.wiley.com/doi/10.1002/3527603433.ch2 by Benjamin Moore - University Of Rhode Island Lib , Wiley Online Library on [04/10/2024]. See the Terms and Conditions (https://onlinelibrary.wiley.com/terms-and-conditions) on Wiley Online Library for rules of use; OA articles are governed by the applicable Creative Commons License

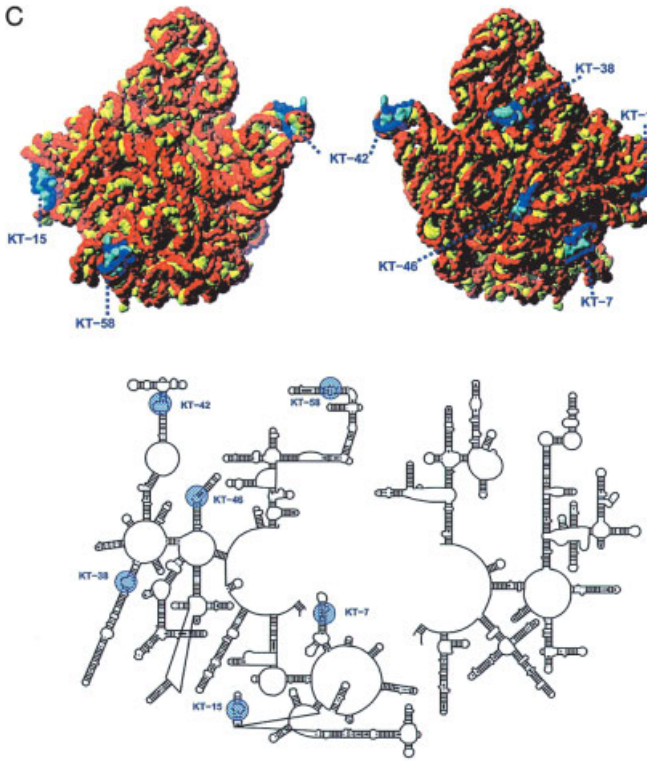

Figure 2-8 cond.

2.6.2.1 **Classification of Lonepair Triloops**

All but one of the LPTLs are coaxially stacked on the nearest 5′-helix. The LPTLs can be classified as directly (class I) or indirectly (mediated by a short helical region (class II)), coaxially stacking LPTLs. In both classes, the 5′-base of the lonepair (F) is stacked onto the first nucleotide of the triloop (X), which is connected to the second nucleotide of the triloop (Y) by a 220–230° U-turn. The second and third nucleotides are facing into the minor groove, with the third base forming hydrogen bonds to the first nucleotide of the triloop (see Figs. 2-9A and B).

In a subpopulation of type I and II LPTLs, a tertiary base is recruited by the triloop by forming a base pair to the first base of the triloop (X). This recruited tertiary base stacks between the third base (Z) and the 3′-base in the lonepair (L) and yields a structural conformation resembling that of the tetraloop motif. In contrast to the above-described type A LPTLs, no tertiary base is recruited by type B LPTLs [81]. A third class of LPTLs includes all LPTLs within a helical region. This category of LPTLs is structurally distinct from the first two classes in having at least two of the triloop bases base-pairing to form part of a regular helical stem and in missing the U-turn

10.1002/3527603433.ch2, Downloaded from https://onlinelibrary.wiley.com/doi/10.1002/3527603433.ch2 by Benjamin Moore - University Of Rhode Island Lib , Wiley Online Library on [04/10/2024]. See the Terms and Conditions (https://onlinelibrary.wiley.com/terms-and-conditions) on Wiley Online Library for rules of use; OA articles are governed by the applicable Creative Commons License

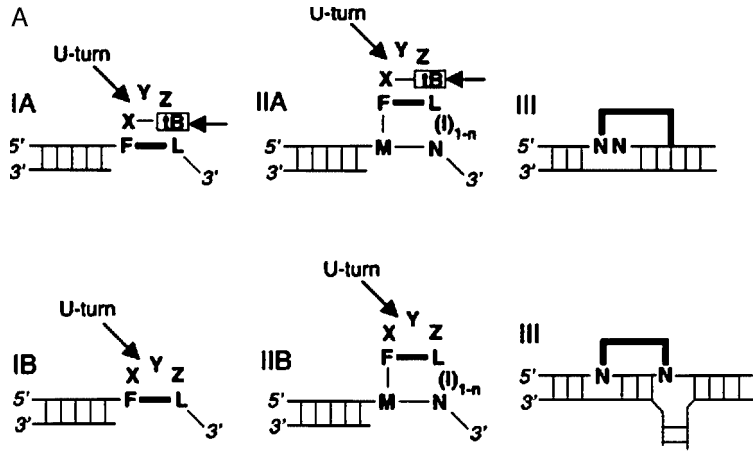

Figure 2-9 Lonepair triloop. (A) Schematic representation of IA, IB, IIA, IIB, and III LPTLs. The lonepair F:L is appended either directly (class I) or indirectly (class II) through the intervening base-pair(s) M:N to its 5′-helix, which is shown with lines (see text for details). (B) Three-dimensional structure of representatives of type IA, IB, and IIA LPTLs. Nucleotides are numbered in black give *T. thermophilus* numbers for 16 S rRNA and *H. marismortui* numbers for 23 S rRNA and in red *E. coli* numbers. From Ref. [81] with permission.

in the triloop [81]. The LPTLs reviewed here include the earlier reported T-loop RNA fold as a type I LPTL [82].

2.6.3 Systemizing Base Pairs

To facilitate the understanding of non-canonical base interactions, which have proven to stabilize secondary and tertiary structures, different groups have put together compilations of non-Watson–Crick interactions. Westhof and colleagues have sorted the base–base interaction by the C1′–C1′ distance and the orientation of the glycosidic bonds. Two base pairs with nearly the same C1′–C1′ distance and same glycosidic bond orientation can replace each other without drastically changing the 3D path and relative geometric orientations of the phosphate-sugar backbones. These base pairs are called isosteric, although they will not always occupy the same volume of space. This collection of isosteric base-pair interactions will be useful in the development of more accurate 3D RNA models.

In the course of this work, Leontis and Westhof [83] systemized the nomenclature of base pairs, based on the three potential hydrogen bond forming edges of a base. These are the Watson–Crick, the Hoogsteen edge for purines and the CH edge for pyrimidines, and the sugar or the shallow groove edge (Fig. 2-10).

10.1002/3527603433.ch2, Downloaded from https://onlinelibrary.wiley.com/doi/10.1002/3527603433.ch2 by Benjamin Moore - University Of Rhode Island Lib , Wiley Online Library on [04/10/2024]. See the Terms and Conditions (https://onlinelibrary.wiley.com/terms-and-conditions) on Wiley Online Library for rules of use; OA articles are governed by the applicable Creative Commons License

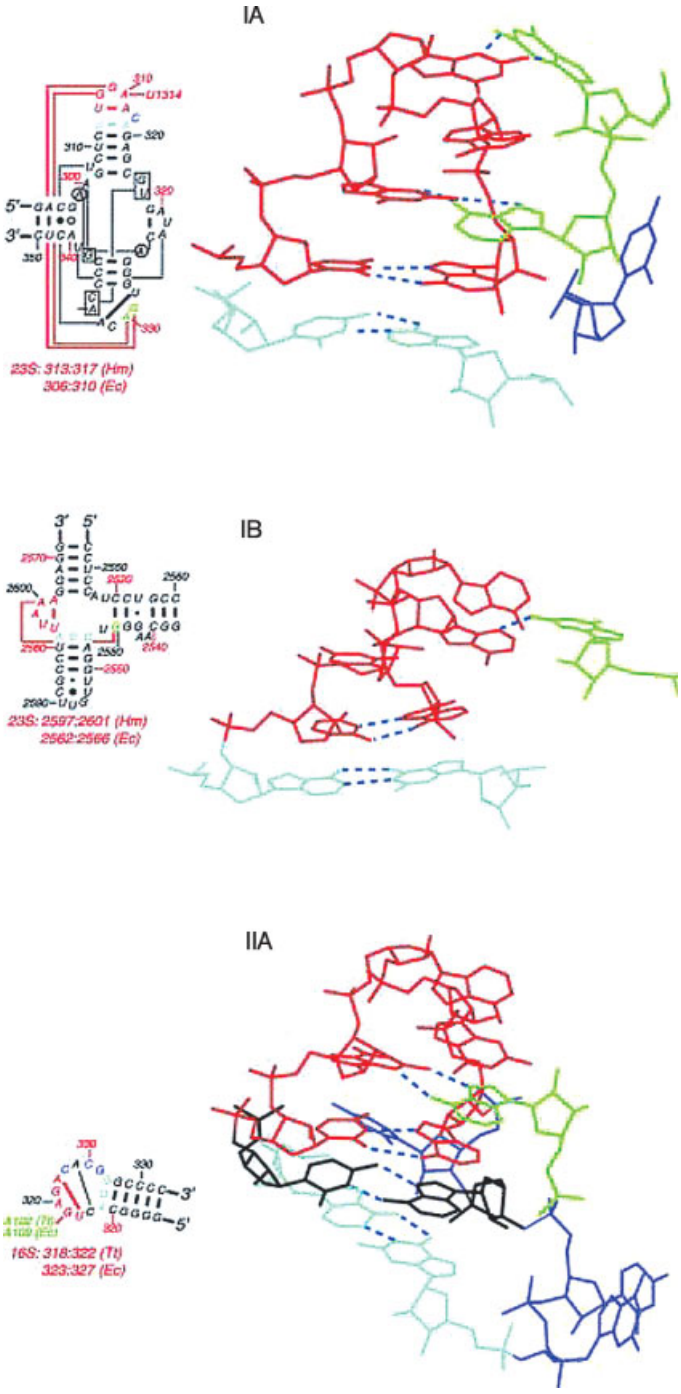

Figure 2-9 (cond.)

10.1002/3527603433.ch2, Downloaded from https://onlinelibrary.wiley.com/doi/10.1002/3527603433.ch2 by Benjamin Moore - University Of Rhode Island Lib , Wiley Online Library on [04/10/2024]. See the Terms and Conditions (https://onlinelibrary.wiley.com/terms-and-conditions) on Wiley Online Library for rules of use; OA articles are governed by the applicable Creative Commons License

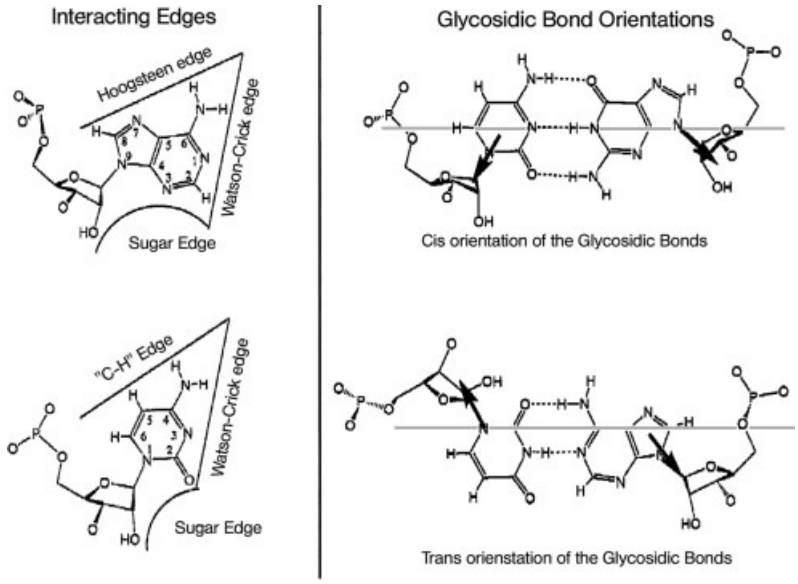

Figure 2-10 Proposed nomenclature for base pairs by Leontis and Westhof. Left panel: purine (A or G, indicated by "R") and pyrimidine (C or U, indicated by "Y") bases provide three edges for interaction, as shown for adenosine and cytosine. Right panel: the *cis* and *trans* orientations are defined relative to a line drawn parallel to and between the *base-to-base* hydrogen bonds in the case of two hydrogen bonds or, in the case of three hydrogen bonds, along the middle hydrogen bonds. From Ref. [83] with permission.

In the NCIR (non-canonical interactions in known RNA structures) database, Fox and colleagues [84] compiled all the RNA structures that contain non-Watson–Crick base–base interactions. In addition, this database provides a summary of the known properties of the base–base interaction (http://prion.bchs.uh.edu/bp_type/).

2.6.4
Systemizing RNA Structural Elements

In their structural classification of RNA (SCOR) database (http://scor.lbl.gov), Fox and colleagues categorized RNA motifs either as an external or internal loop. To define loops, they applied a strict definition for each loop; external loops being a covalently connected series of residues non-Watson–Crick-paired to each other, which are closed on one side by a Watson–Crick base pair, whereas internal loops consist of one (for bulge loops) or two non-Watson–Crick paired residues, closed on both sides by Watson–Crick base pairs. Using their definitions, bulged loops or G•U base pairs within a standard helix are considered internal loops [85]. Two hundred and twenty-three internal and 203 external loops extracted from the 259 NMR and

10.1002/3527603433.ch2, Downloaded from https://onlinelibrary.wiley.com/doi/10.1002/3527603433.ch2 by Benjamin Moore - University Of Rhode Island Lib , Wiley Online Library on [04/10/2024]. See the Terms and Conditions (https://onlinelibrary.wiley.com/terms-and-conditions) on Wiley Online Library for rules of use; OA articles are governed by the applicable Creative Commons License

X-ray structures are complied in the SCOR database. The internal loops are further divided into nine subclasses. The external loops are categorized by size and stacking pattern within the loop. Examples of RNA tertiary interactions are also included in the SCOR database, such as coaxial helical stacking, ribose zippers, A-minor interactions or pseudoknots [85].

2.7 RNA–protein Interactions

The ribosome consists of approximate 53 ribosomal proteins, which are crucial for the smooth functioning of protein synthesis. Therefore, we will turn our attention now to principles governing RNA–protein interaction. We will start by explaining the differences between RNA and DNA and the implication this has for binding protein, which will lead us to the principal modes of interaction between protein and RNA, and ending in the specifics of ribosomal protein interaction with rRNA.

2.7.1 Problem of RNA Recognition

The A-form helix accounts for as much as 50% of the residues in an average non-messenger RNA, which includes the bases of Watson–Crick base pairs as well as G•U wobble base pairs in the runs of Watson–Crick base pairs [66]. In the A-form, the minor groove is shallow and broad (10–11 Å in width and 2.8 Å in depth) whereas the major groove is deep and narrow (4–5 Å in width and 13.5 Å in depth), when compared with B-form helix of DNA (major groove: 12 Å in width and 8.5 Å in depth, minor groove: 5.8 Å in width, 7.5 Å in depth). This allows functional groups of the ribose sugar, in particular the 2′-OH, to participate in interactions. The 2′-OH group can act as a hydrogen bond donor and/or acceptor, making it versatile when it comes to interaction with both RNA and protein. The functional importance of 2′-OH group for protein synthesis was experimentally reinforced in many instances, such as decoding [86], for which the involvement of 2′-OH of the mRNA was structurally rationalized [59], translocation of tRNA(Met) from P-site to the E-site, which is dependent on 2′-OH groups at positions 71 and 76 in the 3′-acceptor arm of the tRNA [87], or tRNA binding to EF-Tu or to aminoacyl-tRNA synthetases [88, 89]

Sequence-specific interactions with regular A-form RNA helices via direct H-bonding and van der Waals interactions *cannot* distinguish, in the minor groove, a G:C from C:G or an A:U from a U:A base pair, but can distinguish G:C from A:U types [90]. This fact degenerates the recognition of base pairs from a quaternary mode (four base pairs) to a binary mode (two kinds of base pairs). This contrasts with the recognition, in the major groove, of B-form DNA where discrimination of all four Watson–Crick base pairs (GC, CG, AT, and TA) is possible (Fig. 2-11; [90]).

This difference in discrimination is reflected in the different mode of sequence-specific recognition of DNA and RNA. DNA recognition is typically accomplished through the recognition of a particular nucleotide sequence in double-stranded DNA (dsDNA). However, the sequence-specific RNA recognition results largely through single-stranded regions, bulges, or internal and terminal loops [91, 92]. The complex

10.1002/3527603433.ch2, Downloaded from https://onlinelibrary.wiley.com/doi/10.1002/3527603433.ch2 by Benjamin Moore - University Of Rhode Island Lib , Wiley Online Library on [04/10/2024]. See the Terms and Conditions (https://onlinelibrary.wiley.com/terms-and-conditions) on Wiley Online Library for rules of use; OA articles are governed by the applicable Creative Commons License

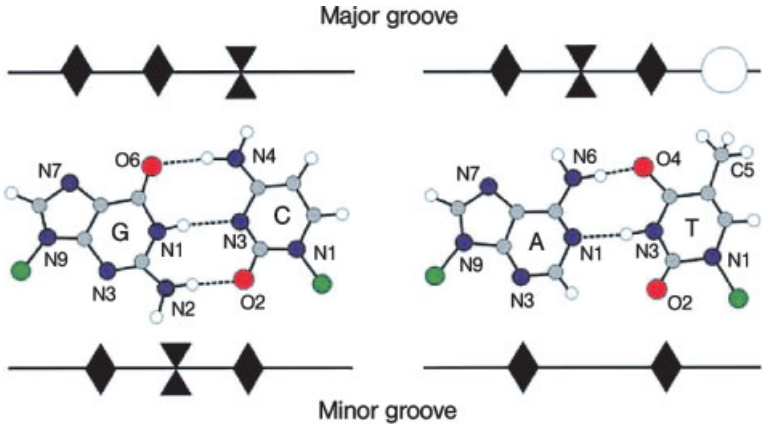

Figure 2-11 A schematic representation of the different patterns of hydrogen-bond donors (two triangles connected on one tip) and acceptors (diamonds) presented by Watson–Crick pairs to the major and the minor grooves. A varied pattern of hydrogen donors and acceptors in the major groove allows easy discrimination of AT, TA, GC, and CG, whereas in the minor groove only the discrimination between AT and GC base pairs is possible due to the symmetric distribution of the donors and acceptors. Adapted From Ref. [90].

structure of the RNA moiety within the protein–RNA complex hampers tight packing at the protein–RNA interface. Therefore, the protein–RNA interface is less well packed in comparison with protein–dsDNA or protein–ssDNA (single-stranded DNA) complexes. Within the protein–RNA complexes, the sequence-specific complexes achieve the best packing with, surprisingly, the least polar protein interface [92].

The difference in sequence-specific recognition of dsDNA and ssRNA also resonates in the hydrogen-bond pattern between amino acids and bases. In dsDNA–protein complexes the functional groups of amino acid side-chains interact with the nucleotide bases in the accessible major groove. In RNA–protein complexes the amide backbone is frequently used for specific base interactions, especially the carbonyl group of the amide group as a proton acceptor. A duplex helix hampers close contact of a peptide backbone with a nucleotide base to a larger extent than ssRNA does. Interestingly, the extent to which an amide group is used for phosphodiester backbone contacts is approximately the same in RNA and DNA complexes [91].

2.7.2
Chemistry of RNA–protein Interactions

In most of the recently published studies on protein–RNA interaction, the structure of *H. marsimortui* 50S is excluded because the constrains of protein–RNA interaction is compounded by the problem of counteracting the high-salt conditions found in *H. marsimortui* cells. A statistical analysis of protein–RNA interactions of the 30S

10.1002/3527603433.ch2, Downloaded from https://onlinelibrary.wiley.com/doi/10.1002/3527603433.ch2 by Benjamin Moore - University Of Rhode Island Lib , Wiley Online Library on [04/10/2024]. See the Terms and Conditions (https://onlinelibrary.wiley.com/terms-and-conditions) on Wiley Online Library for rules of use; OA articles are governed by the applicable Creative Commons License

subunit, synthetase–tRNA complexes and other RNA–protein complexes revealed that 22% of the amino acids in the RNA–protein interface are hydrophobic, 40% charged (positive 32%, negative 8%), 30% polar and 8% glycine. The preferred amino acids at the RNA–protein interface are Arg, Ser, His, Tyr, Lys, with the underrepresented ones being Ala, Val, Glu, Met, Leu, Ile [93]. Statistical analysis has also established that some amino acids have preferences for interacting with either the phosphate group, the ribose moiety or the nucleotide base of the RNA; Arg prefers to interact with the phosphate backbone; Met, Phe and Tyr favor the ribose; Pro and Asn display stronger affinity for bases over ribose or phosphate groups. Additionally, the four bases have individual preferences, such that adenosine favors Ile, Pro, Ser; cytosine, Leu; guanosine, Asp and Gly, and uracil, Asn [93].

2.7.3 rRNA–protein Interaction

Ribosomal proteins make more extensive use of contacts to the sugar-phosphate backbone, which is reflected in the preference for hydrogen bonds to phosphate groups, over ribose, followed by bases. Whereas proteins with sequence-specific binding to ssRNA-like structures make a surprisingly small number of contacts to the RNA backbone and prefer, by far, hydrogen bonds to the base. In-between these two extremes is the tRNA synthetase family, using phosphate, ribose and bases equally for hydrogen-bond contacts [91, 93].

Based on the hypothesis that the ribosome is evolutionary older than tRNA synthetases, which are older than ssRNA–protein complexes, Allers and Shamoo [91] put forward an intriguing idea: They proposed that in the earliest interaction of an "RNA world" RNA-like molecules had only the minimalist chemical interactions with amino acids and therefore would have only take advantage of the abundant peptide backbone amide and carbonyl groups.

The preference of ribosomal proteins to interact with the RNA backbone led to the hypothesis that shape and charge complementarity, rather than specific sequences, are responsible for the specificity observed in ribosomal protein–RNA interactions [75, 76]. This hypothesis is in agreement with co-variation sequence analysis and can also explain the latter's inefficiency in recognizing r-protein binding sites.

As explained above, some of the forces within an RNA–protein complex are understood; however, the understanding of RNA–protein recognition and the mutual interplay between protein and RNA, as seen in the ribosome assembly, is still a long way off [91, 94].

10.1002/3527603433.ch2, Downloaded from https://onlinelibrary.wiley.com/doi/10.1002/3527603433.ch2 by Benjamin Moore - University Of Rhode Island Lib , Wiley Online Library on [04/10/2024]. See the Terms and Conditions (https://onlinelibrary.wiley.com/terms-and-conditions) on Wiley Online Library for rules of use; OA articles are governed by the applicable Creative Commons License

References

1 M. M. Yusupov, G. Z. Yusupova, A. Baucom et al., *Science* **2001**, *292*, 883–996.
2 V. Ramakrishnan, P. B. Moore, *Curr. Opin. Struct. Biol.* **2001**, *11*, 144–154.
3 B. T. Wimberly, D. E. Brodersen, W. M. Clemons et al., *Nature* **2000**, *407*, 327–339.
4 D. E. Brodersen, W. M. Clemons, Jr, A. P. Carter et al., *J. Mol. Biol.* **2002**, *316*, 725–768.
5 N. Nevskaya, S. Tishchenko, M. Paveliev et al., *Acta Crystallogr.* **2002**, *58*, 1023–1029.
6 A. Nikulin, I. Eliseikina, S. Tishchenko et al., *Nat. Struct. Biol.* **2003**, *10*, 104–108.
7 N. Nevskaya, S. Tischenko, R. Fedorov et al., *Struct. Fold. Des.* **2000**, *8*, 363–371.
8 S. Nikonov, N. Nevskaya, I. Eliseikina et al., *EMBO J.* **1996**, *15*, 1350–1359.
9 J. Frank, *Electron Microsc. Rev.* **1989**, *2*, 53–74.
10 H. Stark, F. Mueller, E. V. Orlova et al., *Structure* **1995**, *3*, 815–821.
11 N. Ban, P. Nissen, J. Hansen et al., *Science* **2000**, *289*, 905–920.
12 R. A. Milligan, P. N. Unwin, *Nature* **1986**, *319*, 693–695.
13 A. Yonath, K. R. Leonard, H. G. Wittmann, *Science* **1987**, *236*, 813–816.
14 C. Bernabeu, E. M. Tobin, A. Fowler et al., *J. Cell. Biol.* **1983**, *96*, 1471–1474.
15 P. Dube, M. Wieske, H. Stark et al., *Structure* **1998**, *6*, 389–399.
16 R. Beckmann, D. Bubeck, R. Grassucci et al., *Science* **1997**, *278*, 2123–2126.
17 R. Beckmann, C. M. Spahn, N. Eswar et al., *Cell* **2001**, *107*, 361–372.
18 J. F. Menetret, A. Neuhof, D. G. Morgan et al., *Mol. Cell* **2000**, *6*, 1219–1232.
19 J. Harms, F. Schluenzen, R. Zarivach et al., *Cell* **2001**, *107*, 679–688.
20 P. Nissen, J. Hansen, N. Ban et al., *Science* **2000**, *289*, 920–930.
21 J. Frank, J. Zhu, P. Penczek et al., *Nature* **1995**, *376*, 441–444.
22 I. S. Gabashvili, S. T. Gregory, M. Valle et al., *Mol. Cell* **2001**, *8*, 181–188.
23 T. Tenson, M. Ehrenberg, *Cell* **2002**, *108*, 591–594.
24 C. M. Spahn, R. Beckmann, N. Eswar et al., *Cell* **2001**, *107*, 373–386.
25 J. Greenblatt, *Curr. Opin. Cell Biol.* **1997**, *9*, 310–319.
26 P. S. Lovett, E. J. Rogers, *Microbiol. Rev.* **1996**, *60*, 366–385.
27 D. R. Morris, A. P. Geballe, *Mol. Cell Biol.* **2001**, *20*, 8635–8642.
28 F. Gong, C, Yanofsky, *Science* **2002**, *297*, 1864–1867.
29 M. N. Kazarinoff, E. E. Snell, *J. Biol. Chem.* **1977**, *252*, 7598–7602.
30 M. C. Deeley, C. Yanofsky, *J. Bacteriol.* **1981**, *147*, 787–796.
31 V. Stewart, C. Yanofsky, *J. Bacteriol.* **1986**, *167*, 383–386.
32 F. Gong, C, Yanofsky, *J. Biol. Chem.* **2001**, *276*, 1974–1983.
33 D. Oliver, J. Norman, S. Sarker, *J. Bacteriol.* **1998**, *180*, 5240–5242.
34 H. Nakatogawa, K. Ito, *Mol. Cell* **2001**, *7*, 185–192.
35 H. Nakatogawa, K. Ito, *Cell* **2002**, *108*, 629–636.
36 R. Berisio, F. Schluenzen, J. Harms et al., *Nat. Struct. Biol.* **2003**, *10*, 366–370.
37 A. E. Yonath, J. Mussig, B. Tesche et al., *Biochem. Int.* **1980**, *1*, 428–435.
38 W. M. Clemons, Jr, D. E. Brodersen, J. P. McCutcheon et al., *J. Mol. Biol.* **2001**, *310*, 827–843.
39 F. Schluenzen, A. Tocilj, R. Zarivach et al., *Cell* **2000**, *102*, 615–623.
40 N. Ban, B. Freeborn, P. Nissen et al., *Cell* **1998**, *93*, 1105–1115.
41 I. S. Gabashvili, R. K. Agrawal, C. M. Spahn et al., *Cell* **2000**, *100*, 537–549.
42 D. I. Svergun, M. H. Koch, J. S. Pedersen et al., *J. Mol.Biol.* **1994**, *240*, 78–86.
43 C. M. Spahn, P. A. Penczek, A. Leith et al. *Struct. Fold Des.* **2000**, *8*, 937–948.

10.1002/3527603433.ch2, Downloaded from https://onlinelibrary.wiley.com/doi/10.1002/3527603433.ch2 by Benjamin Moore - University Of Rhode Island Lib , Wiley Online Library on [04/10/2024]. See the Terms and Conditions (https://onlinelibrary.wiley.com/terms-and-conditions) on Wiley Online Library for rules of use; OA articles are governed by the applicable Creative Commons License

44 C. Glotz, R. Brimacombe, *Nucleic Acids Res.* **1980**, *8*, 2377–2395.
45 A. Nakagawa, T. Nakashima, M. Taniguchi et al., *EMBO J.* **1999**, *18*, 1459–1467.
46 M. Worbs, R. Huber, M. C. Wahl, *EMBO J.* **2000**, *19*, 807–818.
47 S. Spillmann, F. Dohme, K. H. Nierhaus, *J. Mol. Biol.* **1977**, *115*, 513–523.
48 A. Yonath, *Curr. Protein Pept. Sci.* **2002**, *3*, 67–78.
49 R. K. Agrawal, J. Linde, J. Sengupta et al., *J. Mol. Biol.* **2001**, *311*, 777–787.
50 M. G. Gomez-Lorenzo, C. M. Spahn, R. K. Agrawal et al., *EMBO J.* **2000**, *19*, 2710–2718.
51 M. Valle, A. Zavialov, J. Sengupta et al., *Cell* **2003**, *114*, 123–134.
52 J. L. Hansen, T. M. Schmeing, P. B. Moore et al., *Proc. Natl. Acad. Sci. USA* **2002**, *99*, 11670–11675.
53 T. M. Schmeing, A. C. Seila, J. L. Hansen et al., *Nat. Struct. Biol.* **2002**, *9*, 225–230.
54 S. V. Kirillov, J. Wower, S. S. Hixson et al., *FEBS Lett.* **2002**, *514*, 60–66.
55 R. R. Gutell, J. C. Lee, J. J. Cannone, *Curr. Opin. Struct. Biol.* **2002**, *12*, 301–310.
56 R. R. Gutell: in *Ribosomal RNA: Structure, Evolution, Processing, and Function in Protein Biosynthesis*, eds R. A. Zimmermann and A. E. Dahlberg, CRC Press, Boca Raton, FL 1996, 111–128.
57 J. Thompson, W. E. Tapprich, C. Munger et al., *RNA* **2001**, *7*, 1076–1083.
58 T. Elgavish, J. J. Cannone, J. C. Lee et al., *J. Mol. Biol.* **2001**, *310*, 735–753.
59 J. M. Ogle, D. E. Brodersen, Jr. W. M. Clemons et al., *Science* **2001**, *292*, 897–902.
60 P. Schimmel, B. Henderson, *Proc. Natl. Acad. Sci. USA* **1994**, *91*, 11283–11286.
61 M. A. Schafer, A. O. Tastan, S. Patzke et al., *J. Biol. Chem.* **2002**, *277*, 19095–19105.
62 D. J. Klein, T. M. Schmeing, P. B. Moore et al., *EMBO J.* **2001**, *20*, 4214–4221.
63 R. T. Batey, R. P. Rambo, J. A. Doudna, *Angew. Chem.-Int. Ed.* **1999**, *38*, 2327–2343.
64 T. Hermann, D. J. Patel, *J. Mol. Biol.* **1999**, *294*, 829–849.
65 N. B. Leontis, J. Stombaugh, E. Westhof, *Biochimie* **2002**, *84*, 961–973.
66 P. B. Moore, *Annu. Rev. Biochem.* **1999**, *68*, 287–300.
67 S. R. Holbrook, S. H. Kim, *Biopolymers* **1997**, *44*, 3–21.
68 W. Saenger: *Principles of Nucleic Acid Structure*, ed. C. R. Cantor, Springer, New York 1984.
69 A. E. Walter, D. H. Turner, *Biochemistry* **1994**, *33*, 12715–12719.
70 A. E. Walter, D. H. Turner, J. Kim et al., *Proc. Natl. Acad. Sci. USA* **1994**, *91*, 9218–9222.
71 J. Kim, A. E. Walter, D. H. Turner, *Biochemistry* **1996**, *35*, 13753–13761.
72 S. E. Lietzke, C. L. Barnes, J. A. Berglund et al., *Structure* **1996**, *4*, 917–930.
73 P. Nissen, J. A. Ippolito, N. Ban et al., *Proc. Natl. Acad. Sci. USA* **2001**, *98*, 4899–4903.
74 J. H. Cate, A. R. Gooding, E. Podell et al., *Science* **1996**, *273*, 1678–1685.
75 G. L. Conn, D. E. Draper, E. E. Lattman et al., *Science* **1999**, *284*, 1171–1174.
76 B. T. Wimberly, R. Guymon, J. P. McCutcheon et al., *Cell* **1999**, *97*, 491–502.
77 D. N. Wilson, G. Blaha, S. R. Connell et al., *Curr. Protein Pept. Sci.* **2002**, *3*, 1–53.
78 M. Tamura, S. R. Holbrook, *J. Mol. Biol.* **2002**, *320*, 455–474.
79 E. A. Doherty, R. T. Batey, B. Masquida et al., *Nat. Struct. Biol.* **2001**, *8*, 339–343.
80 S. K. Silverman, T. R. Cech, *Biochemistry* **1999**, *38*, 8691–8702.
81 J. C. Lee, J. J. Cannone, R. R. Gutell, *J. Mol. Biol.* **2003**, *325*, 65–83.
82 U. Nagaswamy, G. E. Fox, *RNA* **2002**, *8*, 1112–1119.
83 N. B. Leontis, E. Westhof, *RNA* **2001**, *7*, 499–512.

10.1002/3527603433.ch2, Downloaded from https://onlinelibrary.wiley.com/doi/10.1002/3527603433.ch2 by Benjamin Moore - University Of Rhode Island Lib , Wiley Online Library on [04/10/2024]. See the Terms and Conditions (https://onlinelibrary.wiley.com/terms-and-conditions) on Wiley Online Library for rules of use; OA articles are governed by the applicable Creative Commons License

84 U. Nagaswamy, M. Larios-Sanz, J. Hury et al., *Nucleic Acids Res.* **2002,** *30,* 395–397.

85 P. S. Klosterman, M. Tamura, S. R. Holbrook et al., *Nucleic Acids Res.* **2002,** *30,* 392–394.

86 A. P. Potapov, F. J. Triana-Alonso, K. H. Nierhaus, *J. Biol. Chem.* **1995,** *270,* 17680–17684.

87 J. S. Feinberg, S. Joseph, *Proc. Natl. Acad. Sci. USA* **2001,** *98,* 11120–11125.

88 J. A. Pleiss, O. C. Uhlenbeck, *J. Mol. Biol.* **2001,** *308,* 895–905.

89 J. A. Pleiss, A. D. Wolfson, O. C. Uhlenbeck, *Biochemistry* **2000,** *39,* 8250–8258.

90 T. A. Steitz: in *The RNA World : the Nature of Modern RNA Suggests a Prebiotic RNA,* eds R. Gesteland, T. R. Cech and J. Atkins, Cold Spring Harbor Laboratory Press, Cold Spring Harbor, New York 1999, 427–450.

91 J. Allers, Y. Shamoo, *J. Mol. Biol.* **2001,** *311,* 75–86.

92 S. Jones, D. T. Daley, N. M. Luscombe et al., *Nucleic Acids Res.* **2001,** *29,* 943–954.

93 M. Treger, E. Westhof, *J. Mol. Recog.* **2001,** *14,* 199–214.

94 J. R. Williamson, *Nat. Struct. Biol.* **2000,** *7,* 834–837.

95 B. Weisblum, *Antimicrob. Agents Chemother.* **1995,** *39,* 797–805.

96 P. Delbecq, O. Calvo, R. K. Filipkowski et al., *Curr. Genet.* **2000,** *38,* 105–112.

97 P. Fang, Z. Wang, M. S. Sachs, *J. Biol. Chem.* **2000,** *275,* 26710–26719.

98 G. L. Law, A. Raney, C. Heusner et al., *J. Biol. Chem.* **2001,** *276,* 38036–38043.

99 A. L. Parola, B. K. Kobilka, *J. Biol. Chem.* **1994,** *269,* 48497–4505.

100 A. Raney, G. L. Law, G. J. Mize et al., *J. Biol. Chem.* **2002,** *277,* 5988–5994.

101 K. Reynolds, A. M. Zimmer, A. Zimmer, *J. Cell Biol.* **1996,** *134,* 827–835.

102 J. P. Alderete, S. Jarrahian, A. P. Geballe, *J. Virol.* **1999,** *73,* 8330–8337.

103 R. R. Gutell, J. J. Cannone, Z. Shang et al., *J. Mol. Biol.* **2000,** *304,* 335–354.

104 M. Stöffler-Meilicke, G. Stöffler: in *The Ribosome. Structure, Function and Evolution,* eds W. E. Hill, A. Dahlberg, R. A. Garrett et al., American Society for Microbiology, Washington, DC 1990 123–133.

105 J. Frank, R. Agrawal: in *Embryonic Encyclopedia of Life Sciences Nature Publishing Group,* London 1999, www.els.net.

10.1002/3527603433.ch2, Downloaded from https://onlinelibrary.wiley.com/doi/10.1002/3527603433.ch2 by Benjamin Moore - University Of Rhode Island Lib , Wiley Online Library on [04/10/2024]. See the Terms and Conditions (https://onlinelibrary.wiley.com/terms-and-conditions) on Wiley Online Library for rules of use; OA articles are governed by the applicable Creative Commons License